
Senior Projects Spring 2017


Bard Undergraduate Senior Projects

Spring 2017

Modeling purple sea urchin and California sheephead populations in southern California kelp forests

Olivia Rachel Williams
Bard College, ow1310@bard.edu

Follow this and additional works at: https://digitalcommons.bard.edu/senproj_s2017

 Part of the [Ordinary Differential Equations and Applied Dynamics Commons](#), [Plant Sciences Commons](#), [Population Biology Commons](#), and the [Terrestrial and Aquatic Ecology Commons](#)



This work is licensed under a [Creative Commons Attribution-NonCommercial-No Derivative Works 4.0 License](#).

Recommended Citation

Williams, Olivia Rachel, "Modeling purple sea urchin and California sheephead populations in southern California kelp forests" (2017). *Senior Projects Spring 2017*. 355.
https://digitalcommons.bard.edu/senproj_s2017/355

This Open Access work is protected by copyright and/or related rights. It has been provided to you by Bard College's Stevenson Library with permission from the rights-holder(s). You are free to use this work in any way that is permitted by the copyright and related rights. For other uses you need to obtain permission from the rights-holder(s) directly, unless additional rights are indicated by a Creative Commons license in the record and/or on the work itself. For more information, please contact digitalcommons@bard.edu.

Modeling purple sea urchin and California sheephead populations in southern California kelp forests

A Senior Project submitted to
The Division of Science, Mathematics, and Computing
of
Bard College

by
Olivia Williams

Annandale-on-Hudson, New York
May, 2017

Abstract

In this project I am modelling the predator-prey relationship between California sheephead and purple sea urchin populations, respectively, in kelp forests off the coast of southern California. The Lotka-Volterra equations explain predator-prey relationships in their most basic form and are written using the following differential equations: $\frac{dV}{dt} = aV - bVP$, $\frac{dP}{dt} = cVP - dP$, where V and P represent the number of prey and predators respectively, and the parameters are positive and real. These equations incorporate a set of assumptions that can be unrepresentative of many ecological systems. I will consider alternate models that incorporate variations of the Lotka-Volterra model which may better represent the biology of the purple sea urchins and California sheephead. Using biological characteristics of both species in kelp forests, I will set possible and likely parameters and solve for unknown parameters. After constructing the models, I will fit each model to the population data. Once I fit each model to the data, I will compute various error estimations using four possible objective functions and determine the model of best fit.

Contents

Abstract	iii
Acknowledgments	vii
1 Introduction	1
2 Lotka-Volterra and its Variations	5
2.1 Lotka-Volterra Model	5
2.1.1 Equilibrium Solutions	7
2.1.2 Graphical Solutions	8
2.1.3 Model Assumptions	11
2.2 Alternate Models	13
3 Our Paper	21
3.1 Constructed Models	21
3.2 Equilibrium Analysis	22
3.3 Error Estimation	26
4 Channel Islands National Park Kelp Forests	29
4.1 Kelp Forest Monitoring Program	29
4.2 Kelp Forests	32
4.2.1 Ecology of Kelp Forests	32
4.2.2 Establishment	35
4.2.3 Deforestation	36
5 Our Data Set	39
5.1 Significance of Predator-Prey Relationships	39
5.2 Purple Sea Urchins and California Sheephead	40
5.2.1 Purple Sea Urchins	40
5.2.2 California Sheephead	42

5.2.3	California Sheephead and Purple Sea Urchin Predator-Prey Relationship	43
5.3	Population Data	45
5.3.1	Purple Sea Urchins Methods	45
5.3.2	California Sheephead Methods	46
5.3.3	Data Used for Analysis	47
6	Applying known models to our data	51
6.1	Refining Models	51
6.2	Fitting Models to our Data	52
6.3	Error Estimation	62
7	Conclusions	69
7.1	Error Estimation Discussion	69
7.2	Future Work	75
A	Mathematica Notebook: 6.1 Calculations	77
B	Mathematica Notebook: Equilibrium Points	83
	Bibliography	89

Acknowledgments

I would like to thank John Cullinan and Elias Dueker for being supportive and enthusiastic advisers over the past year. I would also like to thank Lauren Rose and Gideon Eshel for encouraging me to pursue my interest in math. Finally I would like to thank Joshua Sprague and the Channel Islands National Park for providing me with the kelp forest data, without which this project would not have been possible, and all those who helped me along this journey.

1

Introduction

The Lotka-Volterra model is a set of differential equations that describes predator-prey relationships over time, where V represents prey abundance and P represents predator abundance. The Lotka-Volterra equations can be expressed as follows:

$$\begin{aligned}\frac{dV}{dt} &= aV - bVP \\ \frac{dP}{dt} &= cVP - dP,\end{aligned}$$

where all parameters are positive rate constants. We will discuss the parameters, equilibrium solutions, graphical solutions, and assumptions of the model in Chapter 2. The Lotka-Volterra set of differential equations predicts periodic cycling of both populations. First, we will give a known example of a predator-prey relationship which resembles the periodic solutions to the Lotka-Volterra model.

One of the most well-documented examples of a predator-prey relationship causing regular cycles in each other's populations is the case of the red grouse, *Lagopus lagopus scoticus* and its nematoid parasite [17]. Their predator-prey relationship is characterized by a host and a parasite [17]. Figure 1.0.1 depicts the change in both populations over time, where we can see both the grouse and nematode populations cycle with an approximate 5 year period. While both populations affect the other, it is important to note that the Lotka-Volterra model significantly

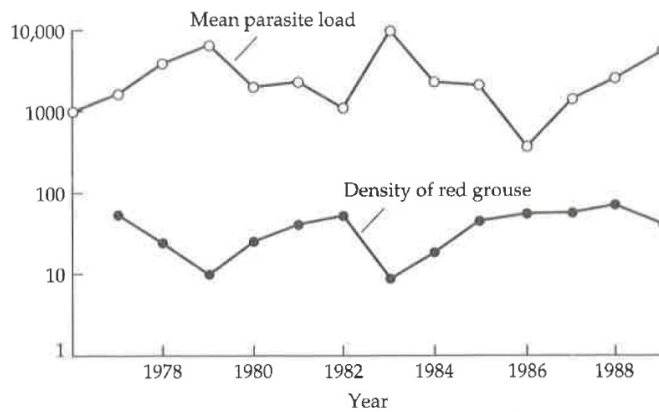


Figure 1.0.1: Red grouse density and mean parasite load per host from 1976-77 to 1989. Data collected at Gunnerside, North Yorkshire. [17].

simplifies the complexity of this relationship. Aside from this case, there are other empirical examples of populations which follow the trends predicted by the Lotka-Volterra model [42].

For the purpose of this paper, we are interested in modeling the predator-prey relationships in Channel Islands kelp forests off the coast of southern California. The Channel Islands National Park Kelp Forest Monitoring (KFM) Program provided us with population data for a variety of algae, invertebrate, and fish species they began collecting data for in 1982. Giant kelp, *Macrocystis pyrifera*, dominate southern California kelp forests, and kelp forests along the Pacific coast in North America [45]. Kelp forests that are home to giant kelp are among one of most dynamic, diverse, and productive ecosystems across the world [18]. Kelp forests provide habitat to myriad biota, including marine mammals, fishes, invertebrates, and other algae [45]. For these reasons, we are interested in studying populations that live within these kelp forests.

In deciding which predator-prey populations to model, we will consider which species are integral to functioning kelp forests. Cited extensively throughout kelp forest literature, sea urchins are important herbivores which influence the structure of kelp forest communities [23]. Kelp grazing by sea urchins has been shown to impact algal assemblage, also causing cascading effects on entire communities [23]. In the Channel Islands specifically, kelp deforestation has occurred due to sea urchin grazing since the long-term monitoring began [18]. The KFM Program supplied us with population data for white, red, and purple sea urchins. Deciding to model sea urchins

as our prey species, we want to select a predator that has been shown to have strong effects on sea urchins.

Sheephead, *Semicossyphus pulcher*, and spiny lobsters, *Panulirus interruptus*, are considered important predators of sea urchins in California kelp forests [5] [19] [33]. Historically, sea otters were important predators of sea urchins as well, but they are now absent from forests throughout California coasts [10]. Abundances, size-frequencies, and spatial distributions have altered due to fishery effects on sheephead and spiny lobster populations in California [10]. The impact of fishing on these two predators has reduced their ecological roles [10]. Studies have specifically researched the effects of sheephead on sea urchins, namely red sea urchins, so for this reason we will focus our paper on the relationship between California sheephead and sea urchins [5] [19]. We created preliminary population abundance figures, plotting each sea urchin species on the x axis and California sheephead on the y axis, and found the figure with purple sea urchins suggested a relationship with and dependence on the sheephead. Choosing between the three sea urchin species to use in our paper, we will focus on the purple sea urchin population.

Now that we have chosen to model on the relationship between California sheephead and purple sea urchin populations, we will begin with the standard Lotka-Volterra model, and then construct different models that incorporate unique biological assumptions. Following the construction of all of our models, we will use two functions, F and ET , to calculate R^2 which indicates the fraction of the total variation explained by each model [34]. The first function, F , represents the objective function which we will present four unique possibilities to use in our analysis [34]. The second function, ET , denotes the considered total variation of the observed data [34]. Finally, we will conclude which models best fit the data, which do not, and confront the future work that we can undergo to accomplish a deeper understanding between of the predator-prey relationship between the California sheephead and purple sea urchin populations.

2

Lotka-Volterra and its Variations

2.1 Lotka-Volterra Model

The Lotka-Volterra model predicts predator and prey population changes over time. Representing the predator population with P and the prey population with V , the growth of the prey population is defined as some function, F , containing both prey and predator numbers [17]:

$$F(V, P) = \frac{dV}{dt}. \quad (2.1.1)$$

Similarly, the predator population can be written as some function, G , where the number of predators is affected by both predator and prey populations [17]:

$$G(V, P) = \frac{dP}{dt}. \quad (2.1.2)$$

Then, we can define the Lotka-Volterra model as the system of differential equations:

$$\begin{aligned} \frac{dV}{dt} &= f(V)V - g(V)P, \\ \frac{dP}{dt} &= i(V)P - j(P)P, \end{aligned} \quad (2.1.3)$$

where $f(V)$ and $j(P)$ are prey and predator intrinsic growth functions, respectively, $g(V)$ is the functional response representing prey consumption by a single predator, and $i(V)$ is the numeric response representing the effect of the functional response on predator population growth [34] [17].

Let's consider the Lotka-Volterra model (2.1.3) in its original and most basic form [4]:

$$\begin{aligned}\frac{dV}{dt} &= rV - \alpha VP \\ \frac{dP}{dt} &= \beta \alpha VP - qP,\end{aligned}\tag{2.1.4}$$

so that

$$\begin{aligned}f(V) &= r \\ g(V) &= \alpha V \\ i(V) &= \beta g(V) \\ j(P) &= q.\end{aligned}\tag{2.1.5}$$

It is important to first note that in Equation 2.1.4, the Lotka-Volterra equations were originally stated using one constant, instead of two, in front of VP in the $\frac{dP}{dt}$ expression [4].

The first term of $\frac{dV}{dt}$ in Equation 2.1.4, rV , represents growth of prey where the positive constant r is the intrinsic rate of increase of prey such that they exponentially increase in the absence of predators [17].

To counterbalance prey positive growth, the second term of $\frac{dV}{dt}$, αVP , represents the loss of prey due to predation which is proportional to the product of predator and prey population values [17], where α quantifies the predator capture efficiency per individual prey [17]. Units of α are $[\text{prey}/(\text{prey} \cdot \text{t} \cdot \text{predator})]$. A large value for α would correspond to an organism that can consume many prey, for instance a filter feeding whale, whereas a small value for α would correspond to an organism that consumes very little prey, such as a web building spider [17].

Next we will discuss the functional response of the predator, $g(V)$, in Equation 2.1.4, but first we will define functional response.

Definition 2.1.1. The functional response of a predator is represented by $g(V)$ and is defined as the rate of prey capture by an individual predator as a function of prey abundance [17] [44].

The functional response comes in three classic forms:

1. Type I functional response
2. Type II functional response

3. Type III functional response

△

In Equation 2.1.4, we have a type I functional response, described as $g(V) = \alpha V$, where α measures capture efficiency and can also be described as discovery rate – taking into account the searching for prey by predators [11]. In the next section we will consider the type II and type III functional responses that contain unique biological assumptions, and examine further variations of these functional responses.

Now let's consider $\frac{dP}{dt}$ in Equation 2.1.4. The second term, $-qP$, represents negative growth, or the number of deaths, of the predator population in the absence of their prey, V , where $j(P) = q$ is the per capita death rate of predators [17]. The first term, $\beta\alpha VP$, represents positive growth of predators in the presence of the prey population, where β is a measure of conversion efficiency [17]. Conversion efficiency is defined as the ability of predators to convert each individual prey into per capita growth rate for the population of predators [17]. Units of β are [predators/(predator*time*prey)] [17]. We expect large values for β when an individual prey is worth a great deal to the predator, such as the value of a moose to wolves [17].

The numeric response of predators is reflected through the $i(V) = \beta g(V) = \beta\alpha V$, where this represents the predator population per capita growth rate as a function of abundance of prey [17].

2.1.1 Equilibrium Solutions

To find the equilibrium solutions for the prey and predator populations in Equation 2.1.4, we set each equation equal to zero and solve for the equilibrium values of V and P , which we denote by V^* and P^* , respectively. In doing so, we will solve for the positive non-zero equilibrium points because we are looking at predator-prey interactions where both populations are present. First,

lets consider $\frac{dV}{dt}$ from this system of differential equations. Setting $\frac{dV}{dt} = 0$, we find:

$$\begin{aligned} 0 &= rV - \alpha VP \\ rV &= \alpha VP \\ r &= \alpha P \\ P^* &= \frac{r}{\alpha}. \end{aligned} \tag{2.1.6}$$

where we see that the prey equilibrium solution is in terms of predators. This means that the prey population at zero growth is controlled by the predator population when it is equal to the ratio of the prey growth rate, r , to the predators capture efficiency, α . In other words, the greater the growth rate of prey, a greater number of predators is needed to maintain prey population at zero growth. On the other hand the greater the capture efficiency, the fewer the number of predators are needed to keep the population growth of prey at zero.

Next, we will solve for V^* by setting $\frac{dP}{dt} = 0$:

$$\begin{aligned} 0 &= \beta\alpha VP - qP \\ \beta\alpha VP &= qP \\ \beta\alpha V &= q \\ V^* &= \frac{q}{\beta\alpha}. \end{aligned} \tag{2.1.7}$$

where we have a specific number of prey necessary to keep predator abundance constant with zero growth. The number of prey to achieve no growth of predators is expressed as the ratio of the predator death rate, q , to the product of predator conversion efficiency, β , and predator capture efficiency, α . This means, the greater the predator death rate, the greater number of prey are needed to keep the prey population from changing. The greater the capture efficiency or the greater the conversion efficiency, however, the fewer prey are needed to maintain a constant predator abundance.

2.1.2 Graphical Solutions

Now that we have the equilibrium solutions for Equation 2.1.4, V^* and P^* , these values are also equivalent to the prey and predator isoclines, respectively. We can graph the isoclines to visualize

how prey and predator populations increase, decrease, and remain constant as a direct effect of either population [17]. To plot the isoclines, we will place prey on the x axis and predators on the y axis, so that we obtain a horizontal prey isocline and a vertical predator isocline [17]. Each isocline will represent the number of one population to keep the other population constant [17].

For the prey isocline, if the predators increase above $P^* = r/\alpha$, the number of prey will decrease, and if the predators decrease below P^* , the number of prey will increase (Figure 2.1.1). By similar analysis, for the predator isocline, if the number of prey increase above $V^* = q/\beta\alpha$, the number of predators will increase too, and if the number of prey increase below V^* , the predator population will also decrease (Figure 2.1.2).

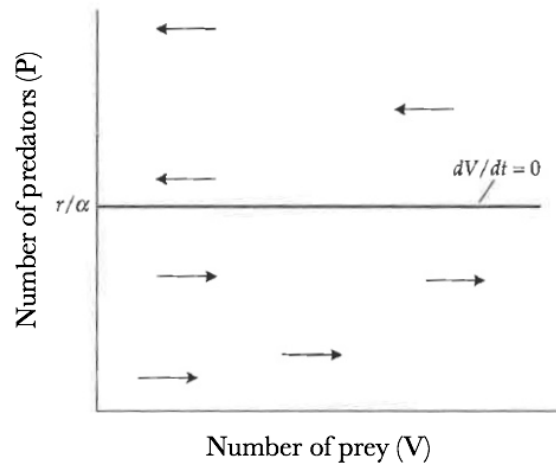


Figure 2.1.1: Prey isocline for Equation 2.1.4. This model states that a certain number of predators, r/α , controls the trajectory of the prey population. When the predator population equals r/α , the prey experience zero growth. If the predator population exceeds r/α , the prey population will decrease (left arrows). Conversely, if the predator population is below r/α , the number of prey increase (right arrows). Figure adapted from [17].

Given our two figures representing the isoclines of each population, prey (Figure 2.1.1) and predator (Figure 2.1.2), where each figure divides the plane into two regions, we can combine both isoclines into one figure creating four distinct regions (Figure 2.1.3). In each region the predator and prey populations experience unique directional changes. This can help us visualize how Equation 2.1.4 predicts the effects of predator and prey populations on the others growth and decline.

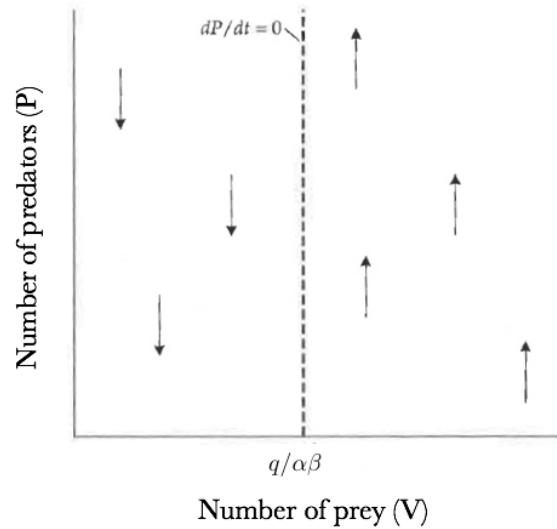


Figure 2.1.2: Predator isocline for Equation 2.1.4. This model states that a certain number of prey, $q/\alpha\beta$, controls the trajectory of the predator population. When the prey population equals $q/\alpha\beta$, the predators experience zero growth. If the prey population exceeds $q/\alpha\beta$, the predator population will increase (upward-pointing arrows). Conversely, if the prey population is below $q/\alpha\beta$, the number of predators decrease (downward-pointing arrows). Figure adapted from [17].

Looking at Figure 2.1.3, in bottom left region, we see that both populations are below the constant number needed to keep the other population constant. In this case, both populations are relatively low which leads to an increase in prey because they experience less pressure from predators. This increase in prey eventually leads to the bottom right region, where there are now more prey and less predators relative to the equilibrium population values. With an increase in prey, predators increase because their food source becomes more abundant, and therefore predators have greater access to food and growth. As the predators increase and prey continue to increase, the populations reach the top right region where there are now a greater number of prey and predators than their equilibrium values. In the top right region, prey begin to decrease because the predators are too abundant and feed on the prey forcing the prey population to decline. This decline of the prey population falls below the predator isocline and leads to the top left region, where predator abundance begins to fall as there are not enough prey for the predators to feed.

Equation 2.1.4, then, predicts the predator and prey populations follow a closed loop in their trajectories over time, depicted in Figure 2.1.3 [17]. This is not the case, however, when

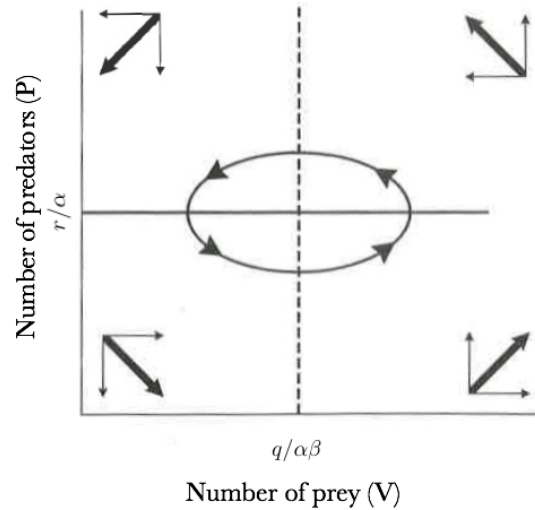


Figure 2.1.3: Phase plane depicting predator and prey isoclines for Equation 2.1.4. In each region, the system of the two populations behaves in a unique way. The vectors demonstrate the course of the populations, where the populations change together to create a cyclical motion. Figure adapted from [17].

both populations are at exactly the equilibrium population depicted by the intersection of the isoclines [17]. At the isocline intersection where $E^* = (V^*, P^*)$, there will be zero growth for both populations.

The closed loop that Equation 2.1.4 predicts the predator and prey populations will follow, provides insight into the characteristics of the growth curves for both populations over time. From the ellipse, we can determine that both populations cycle periodically, where V_{max} occurs when the predator population is at its midpoint, and vice versa [17].

2.1.3 Model Assumptions

While the Lotka-Volterra predator-prey model can predict useful information regarding the trajectory of predator and prey populations, the model carries significant biological assumptions that must be noted. We present the model assumptions of Equation 2.1.4 in the following list, where the first three are standard among other population models, and the last four are specific to Lotka-Volterra in its most simple and basic form (Equation 2.1.4) [17].

- (i) No immigration and emigration: The model only considers births and deaths of the predator and prey populations to change their abundances over time, and assumes immigration is equal to emigration for both species.
- (ii) No age or genetic structure: The model doesn't take into consideration distinct age classes, the most important being the preproductive, reproductive, and postproductive [42] stages. Fecundity rate, or the reproductive rate, depends on age class of the specific species and is not constant across all age groups [8]. The model fails to recognize births as a function of age.
- (iii) No time lags: The model is continuous, and therefore the predator and prey populations respond to one another instantly without delayed effect.
- (iv) Prey growth is exclusively limited by predators: The first term of $\frac{dV}{dt}$ in Equation 2.1.4 demonstrates that regardless of population size, prey grow exponentially at a constant rate of r , in the absence of the predator population [53]. The second term represents death of prey due to consumption by predators.
- (v) The predator is a specialist species and relies only on the prey population to persist: The second term of $\frac{dP}{dt}$ shows that predators die at a constant rate q , in the absence of the one prey population.
- (vi) Predators can consume infinite amounts of prey and find enough prey to consume at any given time: The type I functional response shows that as the number of prey increase, the number of prey consumed per predator increases (Figure 2.2.1) [42].
- (vii) Predator and prey randomly encounter one another in an unvarying, homogeneous environment: The terms, αVP and $\beta\alpha VP$ indicate that the predator and prey populations interact randomly as a function of the product of their abundances and rate constants [17]. These random encounters occur in an environment where the prey do not attain refuges—spatial or temporal – for safety from predators [17].

2.2 Alternate Models

Given the assumptions of Equation 2.1.4, there are a number of model variations we can use in the Lotka-Volterra equations to account for different biological behaviors and assumptions (Equation 2.1.3). In this section, we will look specifically at variations of $f(V)$ and $g(V)$, where whatever changes we make to $g(V)$ will affect $i(V) = \beta g(V)$ (Equation 2.1.3).

Let's start by considering $f(V)$. In Section 2.1 we constructed Equation 2.1.4, where $f(V) = r$, assuming that the prey grow exponentially in the absence of predators. While this assumption may represent certain species in specific systems, some species are limited by carrying capacities of their environments [41]. Incorporating a carrying capacity, k , we can use the logistic growth function for f :

$$f(V) = r \left(1 - \frac{V}{k} \right) \quad (2.2.1)$$

such that

$$\frac{dV}{dt} = r \left(1 - \frac{V}{k} \right) V - \alpha V P. \quad (2.2.2)$$

Recognizing that $V > 0$, as we are considering real, non-extinct populations, then if the carrying capacity is greater than the prey population at a given time step, we have

$$\begin{aligned} k &> V > 0 \\ 1 &> \frac{V}{k} > 0 \\ 1 &> 1 - \frac{V}{k} > 0 \\ 1 &> r \left(1 - \frac{V}{k} \right) > 0. \end{aligned} \quad (2.2.3)$$

This means that the prey population will grow. The closer k and V approach the other while $k > V$, the slower the growth of the prey population. If the prey population at a given time step

is greater than k , then

$$\begin{aligned}
 V &> k \\
 \frac{V}{k} &> 1 \\
 0 &> 1 - \frac{V}{k} \\
 0 &> r\left(1 - \frac{V}{k}\right).
 \end{aligned}
 \tag{2.2.4}$$

Conversely, the prey population will decline. The closer k and V approach the other while $V > k$, the slower the decline of the prey population.

Next, we will consider the variations of $g(V)$. The original Lotka-Volterra model and in its most basic form (Equation 2.1.4) recognizes a type I functional response as discussed in Section 2.1. As stated, the type I functional response assumes that predators can consume an infinite amount of their prey, and that the predator population is a specialist species. The type I functional response also assumes that predators take no handling time [11][17]. The handling time accounts for the time during consumption of each prey per predator [11][17]. Realistically, however, predators do become satiated after feeding upon a threshold of their prey, predators are limited by a handling time, and in many cases, predators are more generalist species where they switch between their choice of prey [11][17].

Given the other biological assumptions which are potentially more realistic for certain systems, we can construct functional responses that are built upon these assumptions. Beginning with the type II functional response, we will address the handling time, catching and consuming prey, of predators. To do so, we will express the type II functional response as a feeding rate, n/t , quantifying the rate an individual predator captures prey, where t is the time spent by a predator feeding on prey, t_s is the search time by a predator for prey, t_h is the handling time by a predator, and n is the total number of prey captured by a predator in time t [17]. We start by stating:

$$t = t_s + t_h. \tag{2.2.5}$$

Then the total handling time, t_h , is equal to the product of the number of prey, n , captured at time t and handling time per prey [17], c :

$$t_h = nc. \quad (2.2.6)$$

Now that we have an expression for handling time (Expression 2.2.6), we can also derive an expression for search time [17]. First,

$$n = V\alpha t_s \quad (2.2.7)$$

where total amount of prey captured by an individual predator, n , is the product of prey abundance, V , the capture efficiency, α , and total search time for prey, t_s [17]. Solving for t_s using division,

$$t_s = \frac{n}{\alpha V}. \quad (2.2.8)$$

Substituting t_s from Expression 2.2.8 and t_h from Expression 2.2.6 into Expression 2.2.5 [17]:

$$t = \frac{n}{\alpha V} + cn. \quad (2.2.9)$$

Multiplying cn by $\frac{\alpha V}{\alpha V}$, we have [17]:

$$\begin{aligned} t &= \frac{n}{\alpha V} + \frac{\alpha V cn}{\alpha V} \\ t &= n \left(\frac{1 + \alpha V c}{\alpha V} \right). \end{aligned} \quad (2.2.10)$$

Solving for the feeding rate, n/t :

$$n/t = \frac{\alpha V}{1 + \alpha V c}. \quad (2.2.11)$$

Now that we have an equation for feeding rate of a predator as a function of the number of prey, and handling time, we can make predictions about the populations and simplify Equation 2.2.11 [17]. If prey abundance is low, the term $\alpha V c$ is low which means the feeding rate will be close to or approximately αV — which is the feeding rate in the original Lotka-Volterra model (Equation 2.1.4) [17]. With a high prey abundance, the feeding becomes closer to the saturation

value, $1/c$, where $1/c$ describes the maximum feeding rate the predator can attain due to the limits of handling time, c [17].

Defining new constants, we let $s = 1/c$, where s now represents the maximum rate of prey consumption per one predator [17] [34]. We also define h as the constant equal to $1/\alpha c$, where h is the half-saturation constant [17] [34]. The half-saturation constant represents the density of prey where the feeding rate is half the maximum [4] [17]. Multiplying each term of Equation 2.2.11, we get:

$$n/t = \frac{\frac{\alpha V}{\alpha c}}{\frac{1}{\alpha c} + \frac{\alpha V c}{\alpha c}}. \quad (2.2.12)$$

Then, substituting s and h into Equation 2.2.12, we find:

$$n/t = \frac{sV}{h + V} \quad (2.2.13)$$

where Equation 2.2.13 represents the type II functional response, yielding a hyperbolic curve (Figure 2.2.1) [17]. We see that the per capita predation rate increases at a decreasing rate as prey population increases until reaching a maximum rate, s , at some prey population size [42].

Next we have the type III functional response, which is represented as:

$$n/t = \frac{sV^2}{h^2 + V^2} \quad (2.2.14)$$

where Equation 2.2.14 yields a sigmoid curve [17] [42]. The per capita predation rate starts low and then increases until reaching a maximum rate, s , as represented by the sigmoid curve (Figure 2.2.1). This maximum rate acts as a horizontal asymptote just as it does in the type II functional response (Equation 2.2.13).

The type III functional response incorporates density dependence at the accelerating region of the sigmoid curve (Figure 2.2.1) [2]. This accelerating region can be described as where the predator switches its prey, and can stabilize a population [2].

There are a few explanations for a type III functional response. First, the predator may be a generalist species, where it switches prey depending on the relative abundance of its preferred prey species [42]. Despite a particular preference for a certain prey species, if that species is

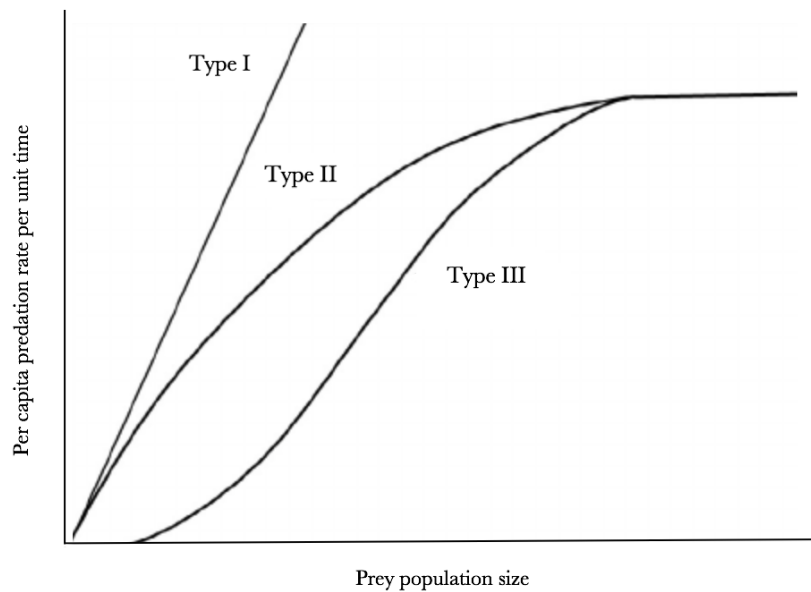


Figure 2.2.1: Graphical representations of the type I, II, and III, functional responses. Type I produces a linear response of per capita predation rate on prey as prey population size increases, type II yields a hyperbolic curve, and type III yields a sigmoidal curve.

low in abundance, the predator will often have a stronger preference for a more abundant prey species, until their preferred species becomes more abundant [42].

Another reason that can result in a type III functional response is availability of cover or refuge that allows prey to escape from predation [42]. If for instance, an environment has limited cover for prey to hide, the refuge will protect a majority of the prey at a low prey population density, but will protect relatively less of the prey as their population increases [42]. This yields low per capita prey consumption by predators when the prey population is low, and a greater per capita prey consumption rate when the prey population is high (Figure 2.2.1).

Finally, another factor that can lead to a type III functional response is a predator's search image [42]. This assumes that a sort of learning behavior occurs in a predator, where when a new prey species is introduced, predation will be low as the predator has not yet learned or recognized this species as food [11] [42]. As the prey population increases, discovery rate and consumption by predators will also increase since they have developed a search image for the prey [11] [42].

Another variation for $g(V)$ specifically takes into account prey refuge. The prey refuge can be included indirectly, like in the type III functional response, but we can include prey refuge in type I functional response, such that:

$$g(V) = \alpha(V - v). \quad (2.2.15)$$

We can also directly include prey refuge in the type II functional response:

$$g(V) = \frac{s(V - v)}{[h + (V - v)]}. \quad (2.2.16)$$

Here, α again measures the capture efficiency, and we now include v where v is the parameter defined as the constant number of prey protected by refuges [34]. Looking first at Equation 2.2.15, The type I functional response with prey refuge is constructed simply as the type I functional response (Expression 3.2.3), but instead of only multiplying the capture efficiency by the number of prey, we multiply capture efficiency by the number of prey subtracted by the number of prey that are protected from predators due to refuges.

Now considering Equation 2.2.16, we use the same logic to construct this functional response. We start by taking the type II functional response (Equation 2.2.13) and subtracting the constant number of prey protected by refuges from the number of prey, such that we arrive at Equation 2.2.16.

For both functional responses incorporating prey refuge, if a habitat consists of many refuges, including rocks, crevices, grasses or any hiding places, that support the prey population at high densities, then v will be high. In this case, per capita consumption rate of prey will decrease and the predator population will not increase at as fast of a rate as it would without prey refuge. This means the prey population will not die off as fast in the presence of refuge. If the refuges in a habitat, however, do not support the prey population at high densities, and can only support few prey, then v will be low and close to zero. In this case the functional response will act close to or the same as the type I and II and functional responses, respectively.

Ratio-dependence assumes that the functional response depends on the ratio of prey to predator population sizes [3]. Ratio-dependence can be expressed as the function $g(V, P)$:

$$g(V, P) = \frac{sV/P}{h + V/P}. \quad (2.2.17)$$

Note that the ratio-dependence functional response is constructed as the type II functional response (Equation 2.2.13), but instead divides V by P . The preceding functional responses, types I, II, and III, and prey refuge functional response, are determined by exclusively one variable – prey abundance [3]. These functional responses that incorporate prey abundance, and not predator abundance, assume that the instantaneous rate of change of the predator population just depends on the instantaneous rate of consumption or kill of prey, which in turn depends on the instantaneous prey density [3] [36]. While these assumptions can hold true in a homogeneous environment where the instantaneous values vary on the same time scale, they do not hold true otherwise [3]. Heterogeneities in environments will induce predator-dependence which the ratio-dependent functional response takes into consideration.

3

Our Paper

3.1 Constructed Models

Beginning with the Lotka-Volterra Model stated in Section 2.1 (Equation 2.1.3), we will use this model as our structural base. To build from the structural base and construct other models, we will incorporate various expressions from population theory, which we defined in Section 2.2, that represent and maintain different biological assumptions (Table 3.1.1) [34].

Table 3.1.1: Expressions to construct models from structural base 1 [34]

Expression	Biological assumptions
1. $f(V) = r$	Exponential growth
2. $g(V) = \alpha V$	Type I functional response
3. $i(V) = \beta g(V)$	Numerical response
4. $j(P) = q$	Constant per capita death rate of the predator population
5. $f(V) = r(1 - \frac{V}{k})$	Logistic growth
6. $g(V) = \frac{sV}{(h+V)}$	Type II functional response
7. $g(V) = \frac{sV^2}{(h^2+V^2)}$	Type III functional response
8. $g(V) \Rightarrow g(V, P) = \frac{sV/P}{(h+V/P)}$	Ratio-dependence type II functional response
9. $g(V) = \alpha(V - v)$	Type I functional response with prey refuge
10. $g(V) = \frac{s(V-v)}{[h+(V-v)]}$	Type II functional response with prey refuge

The parameters used in the expressions in Table 3.1.1 are as follows: r is the prey population intrinsic rate of increase, α is the capture efficiency of predators, β is the food conversion efficiency, q is the predator population per capita death rate, k is the carrying capacity of

the environment, s is the maximum rate of prey consumption per one predator, h is the half-saturation constant, and v is the constant number of prey protected by refuges. While some of the constants are clearly interpreted as defined, others are not and rely on further explanation which we give in Section 2.1 and we will cover later when applying values to each constant.

Given the ten expressions, we can construct twelve unique models, M_i , – each containing different biological assumptions consistent with their populations and environments (Table 3.1.2). Models $M_1 - M_7$ were used in a previous study, and we will consider those as well as models $M_8 - M_{12}$ to model our data [34].

Table 3.1.2: Models constructed for analysis

Model	Differential equations
M_1	$\frac{dV}{dt} = rV - \alpha VP, \frac{dP}{dt} = \beta\alpha VP - qP$
M_2	$\frac{dV}{dt} = r(1 - \frac{V}{k})V - \alpha VP, \frac{dP}{dt} = \beta\alpha VP - qP$
M_3	$\frac{dV}{dt} = rV - \frac{sVP}{h+V}, \frac{dP}{dt} = \frac{\beta sVP}{h+V} - qP$
M_4	$\frac{dV}{dt} = rV - \frac{sV^2P}{h^2+V^2}, \frac{dP}{dt} = \frac{\beta sV^2P}{h^2+V^2} - qP$
M_5	$\frac{dV}{dt} = rV - \frac{sV}{h+V/P}, \frac{dP}{dt} = \frac{s\beta V}{h+V/P} - qP$
M_6	$\frac{dV}{dt} = rV - \alpha(V-v)P, \frac{dP}{dt} = \beta\alpha(V-v)P - qP$
M_7	$\frac{dV}{dt} = rV - \frac{sP(V-v)}{h+(V-v)}, \frac{dP}{dt} = \frac{\beta sP(V-v)}{h+(V-v)} - qP$
M_8	$\frac{dV}{dt} = rV(1 - \frac{V}{k}) - \frac{sVP}{h+V}, \frac{dP}{dt} = \frac{\beta sVP}{h+V} - qP$
M_9	$\frac{dV}{dt} = rV(1 - \frac{V}{k}) - \frac{sV^2P}{h^2+V^2}, \frac{dP}{dt} = \frac{\beta sV^2P}{h^2+V^2} - qP$
M_{10}	$\frac{dV}{dt} = rV(1 - \frac{V}{k}) - \frac{sV}{h+V/P}, \frac{dP}{dt} = \frac{\beta sV}{h+V/P} - qP$
M_{11}	$\frac{dV}{dt} = rV(1 - \frac{V}{k}) - \alpha P(V-v), \frac{dP}{dt} = \beta\alpha P(V-v) - qP$
M_{12}	$\frac{dV}{dt} = rV(1 - \frac{V}{k}) - \frac{sP(V-v)}{[h+(V-v)]}, \frac{dP}{dt} = \frac{\beta sP(V-v)}{[h+(V-v)]} - qP$

3.2 Equilibrium Analysis

Here we will present an equilibrium analysis for each of the twelve possible models described in Section 3.1. For each model M_i , we will first compute the Jacobian matrix, $J_{i(V,P)}$, and evaluate $J_{i(V,P)}$ at the equilibrium points, $E_i^* = (V_i^*, P_i^*)$. Using $J_{i(V,P)}$ evaluated at E_i^* , we will calculate the determinant, $\det J_{i(V^*,P^*)}$, trace, $\text{tr } J_{i(V^*,P^*)}$, and eigenvalues, λ_i . Finally, we will classify

each E_i^* using our findings from the following, where:

$$\lambda_1 = \frac{p}{2} + \frac{\sqrt{p^2 - 4q}}{2}, \quad \lambda_2 = \frac{p}{2} - \frac{\sqrt{p^2 - 4q}}{2}, \quad (3.2.1)$$

such that $\det J_{i(V,P)} = q$ and $\text{tr } J_{i(V,P)} = p$ and we have three cases to consider which are listed below and represented in Figure 3.2.1 [51].

- (i) If $q < 0$, then λ_i are real where $\lambda_1 < 0 < \lambda_2$. We will have *saddle point* at E^* , which is always unstable;
- (ii) If $0 < q < p^2/4$, we will have real roots with same signs. Then for $p > 0$, we find that λ_i are real where $0 < \lambda_1 < \lambda_2$, which means we will have a *source*, which is unstable. If $p < 0$, then we know that $\lambda_1 < \lambda_2 < 0$ and therefore have a *sink*, which is stable;
- (iii) If $q > p^2/4$, then both roots are complex which means we will have oscillations [51]. The sign of p will determine if the amplitude of the oscillation will decrease or increase in time, t [51]. For $p > 0$, we will have a *spiral source*, which is unstable, and for $p < 0$ we have a *spiral sink*, which is stable. Lastly, if $p = 0$, then we have a center point equilibrium, which is neutral [32] [51].

Given the structural base, we begin by computing the partial derivatives of the system of differential equations where,

$$\frac{\partial F}{\partial V} = f'(V) + f(V) - g'(V)P,$$

$$\frac{\partial F}{\partial P} = -g(V),$$

$$\frac{\partial G}{\partial V} = i(V)P,$$

$$\frac{\partial G}{\partial P} = i(V) - j(P) - j'(P)P.$$

Using our partial derivatives we can compute the Jacobian matrix as follows.

$$J_{(V,P)} = \begin{bmatrix} f'(V) + f(V) - g'(V)P & -g(V) \\ i(V)P & i(V) - j(P) - j'(P)P \end{bmatrix}.$$

Now that we have general partial derivatives and a general Jacobian matrix of the structural base, in order to present our data as efficiently as possible, we will now provide a sample calcula-

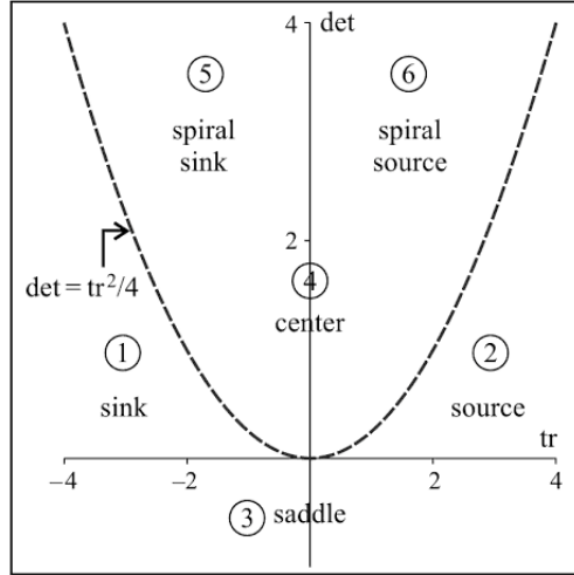


Figure 3.2.1: Trace-determinant plane. Figure obtained from [32].

tion that displays the method used to obtain equilibrium classifications. For each M_i , we display $J_{i(V,P)}$ and E_i^* calculated during our standard procedure used to determine E_i^* classifications in Table 3.2.1.

For our specific example, let's consider M_6 defined by the following system of differential equations,

$$\begin{aligned} \frac{dV}{dt} &= rV - \alpha(V - v)P \\ \frac{dP}{dt} &= \beta\alpha(V - v)P - qP, \end{aligned} \quad (3.2.2)$$

where

$$\begin{aligned} f(V) &= r \\ g(V) &= \alpha(V - v) \\ i(V) &= \beta g(V) \\ j(P) &= q. \end{aligned} \quad (3.2.3)$$

Then for M_6 ,

$$J_{(V,P)} = \begin{bmatrix} r - P\alpha & -\alpha(V - v) \\ P\alpha\beta & -q + \alpha\beta(V - v) \end{bmatrix}. \quad (3.2.4)$$

Table 3.2.1: Jacobian and equilibrium points for constructed models

Model	Jacobian matrix	Equilibrium points
M_1	$J_{1(V,P)} = \begin{bmatrix} r - P\alpha & -V\alpha \\ P\alpha\beta & -q + V\alpha\beta \end{bmatrix}$	$V_1^* = \frac{q}{\alpha\beta}, P_1^* = \frac{r}{\alpha}$
M_2	$J_{2(V,P)} = \begin{bmatrix} r(1 - \frac{k}{V}) + \frac{kr}{V} - P\alpha & -V\alpha \\ P\alpha\beta & -q + V\alpha\beta \end{bmatrix}$	$V_1^* = \frac{q}{\alpha\beta}, P_1^* = \frac{r(-q+k\alpha\beta)}{k\alpha^2\beta}$
M_3	$J_{3(V,P)} = \begin{bmatrix} r - \frac{hsP}{(h+V)^2} & \frac{-sV}{h+V} \\ \frac{hsP\beta}{(h+V)^2} & -q + \frac{sV\beta}{h+V} \end{bmatrix}$	$V_1^* = \frac{-hq}{q-s\beta}, P_1^* = \frac{hr\beta}{-q+s\beta}$
M_4	$J_{4(V,P)} = \begin{bmatrix} r - \frac{2h^2sVP}{(h^2+V^2)^2} & \frac{-sV^2}{h^2+V^2} \\ \frac{2h^2sVP\beta}{(h^2+V^2)^2} & -q + \frac{sV^2\beta}{h^2+V^2} \end{bmatrix}$	$V_1^* = -\frac{h\sqrt{q}}{\sqrt{-q+s\beta}}, P_1^* = -\frac{hr\beta}{\sqrt{q}\sqrt{-q+s\beta}}$ $V_2^* = \frac{h\sqrt{q}}{\sqrt{-q+s\beta}}, P_2^* = \frac{hr\beta}{\sqrt{q}\sqrt{-q+s\beta}}$
M_5	$J_{5(V,P)} = \begin{bmatrix} r - \frac{shP^2}{(hP+V)^2} & \frac{-sV^2}{(hP+V)^2} \\ \frac{shP^2\beta}{(hP+V)^2} & -q + \frac{sV^2\beta}{(hP+V)^2} \end{bmatrix}$	$V_1^* = 0, P_1^* = 0$
M_6	$J_{6(V,P)} = \begin{bmatrix} r - P\alpha & -\alpha(V-v) \\ P\alpha\beta & -q + \alpha\beta(V-v) \end{bmatrix}$	$V_1^* = \frac{q}{\alpha\beta} + v, P_1^* = \frac{r(q+\alpha\beta v)}{\alpha\beta}$
M_7	$J_{7(V,P)} = \begin{bmatrix} r - \frac{hPs}{(h+V-v)^2} & \frac{-s(V-v)}{h+V-v} \\ \frac{hPs\beta}{(h+V-v)^2} & -q + \frac{s\beta(V-v)}{h+V-v} \end{bmatrix}$	$V_1^* = \frac{-hq+qv-s\beta v}{q-s\beta}, P_1^* = \frac{-hqr\beta+qr\beta v-rs\beta^2 v}{q(q-s\beta)}$
M_8	$J_{8(V,P)} = \begin{bmatrix} r - \frac{2rV}{k} - \frac{hPs}{(h+V)^2} & \frac{-sV}{h+V} \\ \frac{hPs\beta}{(h+V)^2} & -q + \frac{sV\beta}{h+V} \end{bmatrix}$	$V_1^* = -\frac{hq}{q-s\beta}, P_1^* = -\frac{hr\beta(hq+kq-ks\beta)}{k(q-s\beta)^2}$
M_9	$J_{9(V,P)} = \begin{bmatrix} r - \frac{2rV}{k} - \frac{2h^2PsV}{(h^2+V^2)^2} & \frac{-sV^2}{h^2+V^2} \\ \frac{2h^2PsV\beta}{(h^2+V^2)^2} & -q + \frac{sV^2\beta}{h^2+V^2} \end{bmatrix}$	$V_1^* = -\frac{h\sqrt{q}}{\sqrt{-q+s\beta}}, P_1^* = \frac{hr\beta(h + \frac{k\sqrt{-q+s\beta}}{\sqrt{q}})}{k(q-s\beta)}$ $V_2^* = \frac{h\sqrt{q}}{\sqrt{-q+s\beta}}, P_2^* = \frac{hr\beta(h - \frac{k\sqrt{-q+s\beta}}{\sqrt{q}})}{k(q-s\beta)}$
M_{10}	$J_{10(V,P)} = \begin{bmatrix} r - \frac{2rV}{k} - \frac{hP^2s}{(hP+V)^2} & \frac{-sV^2}{(hP+V)^2} \\ \frac{hP^2s\beta}{(hP+V)^2} & -q + \frac{sV^2\beta}{(hP+V)^2} \end{bmatrix}$	$V_1^* = -\frac{hq}{q-s\beta}, P_1^* = -\frac{hr\beta(hq+kq-ks\beta)}{k(q-s\beta)^2}$
M_{11}	$J_{11(V,P)} = \begin{bmatrix} r - \frac{2rV}{k} - P\alpha & -\alpha(V-v) \\ P\alpha\beta & -q + \alpha\beta(V-v) \end{bmatrix}$	$V_1^* = \frac{q}{\alpha\beta} + v, P_1^* = -\frac{r(q+\alpha\beta v)(q+\alpha\beta(-k+v))}{kq\alpha^2\beta}$
M_{12}	$J_{12(V,P)} = \begin{bmatrix} r - \frac{2rV}{k} - \frac{hsP}{(h+V-v)^2} & \frac{-s(V-v)}{h+V-v} \\ \frac{\beta hsP}{(h+V-v)^2} & -q + \frac{s\beta(V-v)}{h+V-v} \end{bmatrix}$	$V_1^* = \frac{hq}{-q+s\beta} + v,$ $P_1^* = -\frac{r\beta(hq+(q-s\beta)(k-v))(hq-qv+s\beta v)}{kq(q-s\beta)^2}$

Solving for E^* we determine $V^* = \frac{q}{\alpha\beta} + v$ and $P^* = \frac{r(q+\alpha\beta v)}{q\alpha}$. Therefore evaluating $J_{(V,P)}$, from Expression 3.2.4, at E^* we find:

$$J_{(V^*,P^*)} = \begin{bmatrix} -\frac{r\alpha\beta v}{q} & -\frac{q}{\beta} \\ \frac{r\beta(q+\alpha\beta v)}{q} & 0 \end{bmatrix} \quad (3.2.5)$$

where $\det J_{(V^*,P^*)} = r(q+\alpha\beta v)$, $\text{tr } J_{(V^*,P^*)} = -\frac{r\alpha\beta v}{q}$ and $\lambda_1 = \frac{-r\alpha\beta^2 v - \sqrt{r\beta^2(-4q^3 - 4q^2\alpha\beta v + r\alpha^2\beta^2 v^2)}}{2q\beta}$, $\lambda_2 = \frac{-r\alpha\beta^2 v + \sqrt{r\beta^2(-4q^3 - 4q^2\alpha\beta v + r\alpha^2\beta^2 v^2)}}{2q\beta}$. It is given that all model constants are positive non-zero real numbers. This means $\det J_{(V^*,P^*)}$ is positive because the sum and product of positive real numbers is also a positive real number. By similar reasoning, we also know that $\text{tr } J_{(V^*,P^*)}$ is negative because the product of positive real numbers multiplied by -1 is a negative real number. Since there exists a positive $\det J_{(V^*,P^*)}$ and negative $\text{tr } J_{(V^*,P^*)}$, then the solutions to the ODE must be either a sink or spiral sink [32]. To determine the exact solution and characteristic of E^* , we must consider λ_i . If the value under the radical of λ_i is negative, then our solutions are complex and we have a spiral sink [32]. If the value under the radical of λ_i is positive, then our solutions are real and positive and we have a sink [32].

3.3 Error Estimation

To calculate the model of best fit, we will use four objective functions used in literature representing “(1) the sum of the squared deviations, (2) the sum of the relative squared deviations, (3) the sampling standard deviation of prey as a weight of the deviation of the predators and the converse,” and (4) a chi-squared test [34] [22]. For objective function 3, we use wording consistent with [34], but we will use the unweighted sampling standard deviations. Using objective functions avoids priority for any group, predator or prey, when fitting the models to the data [34]. While others use the results from the objective functions from only the original Lotka-Volterra predation model to determine the best function for further analysis, M_1 , we will run each objective function for all constructed models for comparison purposes. The four objective functions constructed are as follows:

$$F = \begin{cases} F_{of1} = \sum_{n=1}^n [(V_{obs_i} - V_{est_i})^2 + (P_{obs_i} - P_{est_i})^2], \\ F_{of2} = \sum_{n=1}^n \left[\left(\frac{V_{obs_i} - V_{est_i}}{V_{obs_i}} \right)^2 + \left(\frac{P_{obs_i} - P_{est_i}}{P_{obs_i}} \right)^2 \right], \\ F_{of3} = \sum_{n=1}^n F_i = \sum_{n=1}^n \{ [\omega_v (V_{obs_i} - V_{est_i})]^2 + [\omega_P (P_{obs_i} - P_{est_i})]^2 \} \\ \frac{\omega_v}{\omega_P} = \frac{\sigma_P}{\sigma_v} \Rightarrow \omega_P = 1 \therefore \omega_v = \frac{\sigma_P}{\sigma_v}, \\ F_{of4} = \sum_{n=1}^n \left[\frac{(V_{obs_i} - V_{est_i})^2}{V_{obs_i}} + \frac{(P_{obs_i} - P_{est_i})^2}{P_{obs_i}} \right], \end{cases}$$

where F_{of1} is the objective function 1, F_{of2} is the objective function 2, F_{of3} is the objective function 3, and F_{of4} is the objective function 4, n is the total number of data points over time, V_{obs} and P_{obs} are the observed density of prey and predators, respectively, V_{est} and P_{est} are the estimated density of prey and predators, respectively, and σ_v and σ_P are the sampling standard deviations of prey and predator populations, respectively [34]. We will let $\omega_v = 1$, as we are considering the unweighted sampling standard deviations.

To determine the model of best fit, we must calculate the percent of explanation of the unweighted total variation for each model using the following:

$$\begin{aligned} ET &= \sum_{n=1}^n \{ [\omega_v (V_{obs_i} - \bar{V})]^2 + [\omega_P (P_{obs_i} - \bar{P})]^2 \}, \\ R^2 &= \frac{ET - F}{ET}, \end{aligned} \tag{3.3.1}$$

where ET represents total variation, and \bar{V} and \bar{P} are the mean densities of prey and predators, respectively [34]. We can use R^2 as a method for model comparison, where R^2 provides an indication of the fraction of the unweighted total variation accounted for by each specific model [34].

4

Channel Islands National Park Kelp Forests

4.1 Kelp Forest Monitoring Program

Channel Islands National Park (CINP), established in 1980 and located in Ventura, California, contains five islands, including their surrounding ocean [30]. Located beneath the ocean surface and surrounding all the parks islands reside kelp forests, providing shelter for more than 1,000 animal and plant species [30]. Furthermore, kelp forests comprise the CINP with one of their largest and most threatened and complex ecosystems across the parks ocean waters [25]. The CINP and the Channel Islands National Marine Sanctuary are home to one third of all the kelp forests in southern California [30].

In 1982, CINP established the Kelp Forest Monitoring, KFM, Program in an effort to learn the health and continual status of the kelp forests, record environmental changes over time, and establish protective management strategies [30]. To achieve their goals, the monitoring program collects abundance and size data for 70 taxa of fish, invertebrates, and algae – all of which are ecological indicators [25]. Species were selected for long-term monitoring using the following criteria:

1. referenced to in the CINP's permitting legislation or protected by the law,
2. native to the park, or restricted in geographical spread,

3. invasive to the park,
4. exceedingly common or an important characteristic of an entire community,
5. harvested legally,
6. well known or well liked,

supplying an original list of 15 algae, 38 invertebrate, and 15 fish taxa [25]. Over the years of monitoring, the list has slightly changed to now incorporate 16 algae, 41 invertebrate, and all identifiable fish – which as of 2011 incorporates 113 fish species [25]. The monitored species range from extremely abundant and pervasive, to low densities with wide distributions [25]. Many monitored species have life spans ranging from 10 to 50 plus years [25]. Due to the long-living nature of many of the species, their abundances supply a steady measure of environmental conditions within the kelp forest [25].

Obtaining population data for all the species the CINP monitors, allows us to look at relationships between species and try to detect short and long-term changes in the kelp forests. The KFM Program provides us with a mechanism of monitoring the population dynamics, health, and potential human impacts in California kelp forests.

The KFM Program has collected data at 37 sites, 16 of which were established as the monitoring program began in 1981 [25]. The original 16 sites are located across the following five islands: San Miguel, Santa Rosa, Santa Cruz, Anacapa, Santa Barbara (Figure 4.1.1) [25]. In the 80s, few sites were added at those islands and in 2002 and 2003, the program established sites at San Clemente Island (Figure 4.1.1) [25].

The selected sites reflect the biological assemblages and the expansive range of conditions in the park [25]. The park lies at the boundary between the Oregonian province and the Californian province – to the north and south, respectively [25]. Northern waters flow south by California currents, surrounding the western islands of the park, San Miguel and Santa Rosa [25]. The waters of the western islands, therefore, echo the biological assemblages found in the waters of the Oregonian province [25]. The eastern islands, Anacapa and Santa Barbara, contain waters

from the south brought up along the coast [25]. These waters support the biological assemblages of the Californian province – including characteristics of warm temperate biota [25]. At the boundary of the two provinces is Santa Cruz Island, where the waters are characterized by a broad transition zone containing biota from both provinces [25]. These interactions between the plants and animals from both provinces creates an assemblage of species which may be adaptable to varying conditions present in transition zones [25]. Existing wind patterns also affect the marine communities [25]. Northern winds hit the northern coasts of the islands, while the south sides remain mostly sheltered [25].



Figure 4.1.1: Map of the Channel Islands National Park which includes which includes San Miguel, Santa Rosa, Santa Cruz, Anacapa, and Santa Barbara islands. San Clemente is not an island included in the parks boundaries.

When the KFM Program chose initial sites for monitoring, they did not have access to benthic maps indicating kelp persistence, therefore they chose their sites using the following method. Deploying divers to the ocean floor at a chosen depth, they reeled out a 100m long tape [25]. They selected sites if the tape covered 80m of rocky bottom and the reef was not less than 100m [25]. The original 16 sites represent kelp forests across the north and south sides of the each island, and transition zones [25]. Depths of each site range from 4-18m [25].

4.2 Kelp Forests

Kelp forests, constructed out of a variety of kelp species, are found in waters across the world [9] [45] [46]. For the purpose of this study, however, we will discuss the broad ecology of kelp forests worldwide, focusing on the ecology of southern California kelp forests more specifically – as our data were collected in the kelp forests off the southern California coast.

4.2.1 Ecology of Kelp Forests

Kelp forests persist in cold-water, shallow rocky coasts across the world [9] [45] [46]. Members of the Laminariales order, primarily brown algae, make up the structure of kelp forests, creating the largest structures produced by living organisms located in benthic marine ecosystems [9] [45] [46]. Kelp forests are comprised of kelps and their myriad biota, including marine mammals, fishes, invertebrates, and other algae [45].

Kelp genera vary geographically, and can be divided into three morphological groups, or guilds, based on frond canopy height, defined as the canopy, stipitate, and prostrate groups. [45] [46]. The largest kelps which yield floating canopies are ‘canopy’ kelps [45]. The most dominant and largest of canopy kelps is the giant kelp, *Macrocystis* spp., which is prevalent across North and South America’s west coasts, growing up to 45m in height [45]. Giant kelp also dominate kelp forests at dispersed sites across the South Pacific Ocean [45]. *Nereocystis leutkeana*, is among one of the smaller canopy kelps spanning from Central California to Alaska [45]. Other smaller canopy kelps, including *Ecklonia maxima* and *Alaria fistulosa*, are found in South Africa and in Alaska and the Asian Pacific Coast, respectively [45]. These smaller canopy kelp species grow to approximately 10m [45]. The other guilds, stipitate and prostrate kelps predominantly include several species of *Laminaria* sp., *Ecklonia*, *Lessonia*, *Pterygophora*, *Eisenia*, *Pleurophycus*, and *Thalassiophyllum*, and certain species of *Laminaria*, respectively. Figure 4.2.1 shows the dominant kelp species of each region where kelp forests persist.

In terms of taxonomy, kelps alone are not diverse [45]. Kelp forests off the coast of California consist of the most diverse kelp flora compared to kelp forests worldwide [45]. Although these

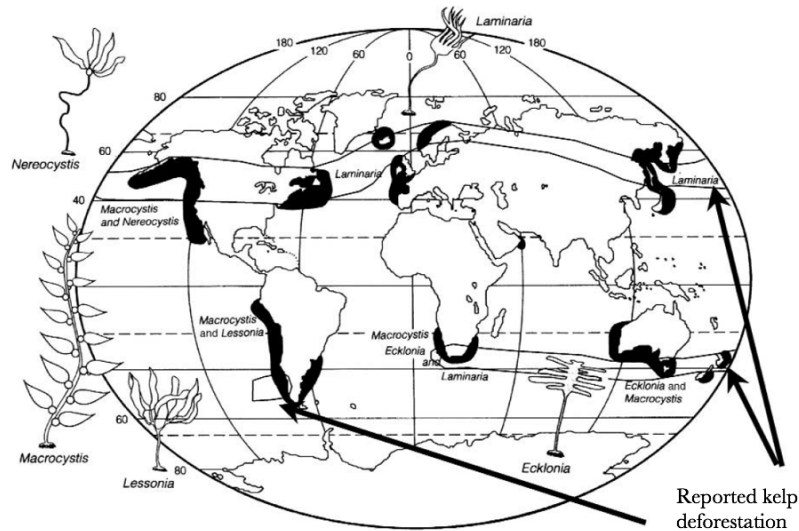


Figure 4.2.1: Distribution of kelp forests across the world, and their corresponding genera. Original figure from Raffaelli and Hawkins, 1996 with marks of deforestation by Steneck, 2002 [45]

kelp forests are the most diverse in kelp flora, they only have 20 kelp species allocated between 16 genera [45]. Most kelp genera are monotypic, meaning each genus includes one species, which explains the proportion of kelp species to genera [45]. Structurally and functionally, kelps are greatly diverse, where their morphology differs within and among genera [45]. Contributing to their morphological diversity, kelps have specialized cells for translocation [45]. Difference in morphology can be seen within each guild, where each guild corresponds to a distinct level of growth in frond length [45]. In canopy forms, kelp fronds grow to the surface where they float, in stipitate forms, fronds inhabit intermediate depths, and in prostrate forms, fronds stay within or near the benthos [45]. Each morphological group can coexist, providing food and habitat for species associated with each group, which together promotes diversity in kelp forest ecosystems [45].

The structure of kelp canopies impacts and influences the local environment through the canopies interactions with biotic and abiotic factors. The structure of kelp forests supplies a multitude of organisms with habitat, food, and nursery ground [45]. Among the kinds of species which inhabit kelp forests, predatory fish can use kelp canopies as habitat [45]. A decrease in canopy, therefore, can lead to a decline in predatory fish, increasing prey and prey larvae sur-

ivorship [45]. Kelp canopies also reduce light in their understory, creating favorable conditions for those species which persist in low light environments [45]. Considering light, then, as a limiting factor, canopy cover can cause interspecific competition among understory algae [45]. A decrease in canopy can change the favorable conditions in the understory for certain species over others. Finally, kelp canopies reduce the amplitude of waves, altering water flow and influencing a number of processes including recruitment, benthic primary and secondary productivity, coastal erosion, and sedimentation [12] [45]. A change in canopy cover, therefore, can influence predator-prey relationships and abundances, the community structure, and environmental conditions.

While kelp forests are highly productive, they are also subject to frequent disturbances [45]. For these reasons, kelp forests have short life cycles [45] [46]. This is one important attribute which is unique to kelp forests in comparison to their terrestrial counterpart—consisting of predominately angiosperm and gymnosperm trees [45]. Kelp forests have shorter average lifespans and structural heights than terrestrial forests [45]. Within 1-3 years, kelp forests attain canopy heights of 1-15 m, where individual kelps can live up to approximately 25 years [45]. In mature terrestrial forests, however, within 20 to 30 years the canopy reaches around 10-30 m, where individual trees can live for centuries to thousands of years [45]. While the longevity and growth of kelp forests are less than terrestrial forests, kelp forests are both more productive and diverse, at the phyla level [45] [46].

The ephemeral nature of kelp forests is complemented by the quickness in which deforestation and re-establishment can occur [45]. Thermal events, such as El Niño events, storms, or surges in herbivorous species can lead to the disappearance of entire kelp beds within one year [45]. After these events which remove and leave no trace of kelp beds, the entire community can reappear in the same time it took for their elimination [45]. Kelp forests persist in a state between their establishment and deforestation, which we will discuss in the following subsections.

4.2.2 Establishment

Kelp forests grow off coasts in shallow rocky cold-waters in a mid-latitude band where light, temperature, and other conditions allow for kelp establishment (Figure 4.2.1) [45]. This mid-latitude band spans approximately 40-60°, north and south of the equator, where light is a limiting factor above 60°, creating strenuous conditions for kelp (Figure 4.2.1) [45]. Above 60°, then, kelp rarely establish [45]. Just as light is a limiting factor preventing the development of kelp forests, warm temperatures and low nutrient concentrations also limit kelp establishment [45]. These factors prevent the development of kelp forests in subtropical and tropical regions, depicted in Figure 4.2.1 [45]. Kelps beds that establish at the lowest latitudes, usually less than 40° latitude, generally correlate with rare ocean currents which bring cool, or cool, nutrient rich waters to warm and/or low nutrient waters [45].

The Channel Islands National Park is at approximately 34° latitude, where we must consider its range to be a little above and below 34° N because the string of islands have varying latitudinal positions. We must consider, therefore, the development of kelp forests at the latitudes between 33° and 35° N. At these lower latitudes, kelp are frequently smaller and have to compete to share the space with fucoids, including large brown algae like *Sargassum*, which grow more prevalent moving toward the tropics [45]. Often times kelps are able to share the space with fucoids, but other times kelp lose their dominance [45]. Along the North American coast, southern California kelps occupy their habitat with fucoids [45]. From 40 – 30°, southern California kelps share areas with *Cystoseira osmundacea*, and from 35 – 25°, *Sargassum* spp. [45]. The KFM Program monitors *Cystoseira* spp and *Sargassum horneri*. annually, along with other green, brown, and red algae species [25].

Now that we have established the range in which kelp can develop, we will focus on the three interacting processes – recruitment, growth, and competition – that generally control establishment of kelp forests [45]. On the local level, kelp forests persist by successful zygote settlement and growth [45]. During the growth process of their benthic life, some zygotes survive while others die due to intraspecific competition [45]. Environmental conditions at the settlement time

affect recruitment, which is usually a seasonal process [45]. After extreme storm events that lead to deforestation, recruitment is often strong [45]. The kelp species that regrow and become dominant in their community, however, depend upon environmental conditions at the time of regrowth [45]. Re-establishment after storm events, therefore, can produce kelp communities with different community structures than prior to deforestation. Kelp forests which consist of multiple morphological groups (Section 4.2.1), have a variety of kelp length levels. In these complex forests, nutrient availability and light availability, created through canopy breaks, controls kelp recruitment and growth [35] [45].

Next, the interactions between nutrient availability, temperature, and light, affect kelp growth [45]. Kelp plants have been observed to erode faster than they grow in the joint effects of high rates of respiration and low nutrient availability, which both correspond to warm water temperatures [45]. Southern California kelp forests rely on the upwelling of new nitrogen to receive sufficient amounts of nutrients [45] [48]. In these kinds of systems, when El Niño events occur they disturb coastal upwelling, which warms surface temperatures, depriving kelp of nutrients and increasing their mortality [46] [50].

In general, the rate at which kelps photosynthesize is relatively low compared to their biomass [45]. This restricts kelps to shallow and well lit areas in comparison to other algal functional groups [52].

4.2.3 Deforestation

Deforestation occurs due to multiple factors, the most notable factors being physiological stress, disease, and herbivory or interactions among any of those methods of deforestation [45]. At different latitudes, kelp forests are more vulnerable to specific processes of deforestation. As we discussed Section 4.2.2, many kelp forests at the lowest latitudes persist due to ocean currents from higher latitudes flowing down to warm temperature waters [45]. At these lower latitudinal ($< 40^\circ$) sites, then, periodic deforestation results from irregular changes in temperature, nutrients, or salinity, killing kelps directly or causing disease [45]. At mid latitudes ($30^\circ - 40^\circ$), deforestation is most common as a result of herbivory by sea urchin [45].

As mentioned in Section 4.2.2, El Niño events cause kelp deforestation [45]. Particularly intense El Niños prevent coastal upwelling, increasing surface water temperature [45]. In California, these warming events triggered patchy deforestation leading to a quick recovery [45] [47] [49]. Their quick recovery can be explained by the diversity and complexity of the kelp forests in southern California [45]. Physiological stresses caused by warming events, as well as storms, may make kelps more vulnerable to widespread disease [45].

While physiological stresses due to changes in temperature, light, and nutrients can cause mortality or disease of kelps, urchin grazing is the dominant and effective form of deforestation in mid-latitudes [9] [14] [45]. Herbivory by urchins can cause long-lasting deforestation, where once an area has been deforested, urchins even under the pressure of predators continually graze and reduce the ability for forests to reestablish [14].

5

Our Data Set

5.1 Significance of Predator-Prey Relationships

Predation is defined as the consumption of a living organism by another, where it can be generally classified into three groups: carnivory – the consumption of animal tissue, herbivory – the consumption of algal or plant tissue, and omnivory – the consumption of animal and plant tissues [42].

Predator-prey relationships are one of the most prominent topics in ecology [4]. It is such a dominant theme because predation is one of the most crucial forces acting in a community, where it is one of the main factors affecting the structure of most ecosystems [16] [31]. Through the direct effect of consuming their prey, predators can reduce or regulate their prey populations [42]. Similarly, prey availability may act as a tool for predator regulation [42]. Not only do the presence of predators cause direct effects on their prey, but their presence also causes indirect effects on their prey populations [31].

Predator presence affects prey populations, where individual decisions made by both the predators and prey populations can affect impacts of predators on prey– creating cascading effects on community and population dynamics [31]. These effects can occur through indirect effects, which can happen when one species impacts another species through one or more intermediate species, where there are multiple types of indirect effects [27] [40]. First, there are

density-mediated indirect effects which cause cascading effects such that an indirect mutualism exists between predators and plants due to the predators fatal consumption of herbivores [27] [40]. A second type of indirect effect is known as a trait-mediated indirect effect [40]. This occurs when one species alters the manner in which two other species interact [40]. An example of a trait-mediated indirect effect is when a trophic cascade occurs from a nonfatal direct effect, for instance, change in prey diet or habitat choice as a result of increased predation risk [40]. A predators consistent diet, or change in prey size, diet, or habitat choice, therefore, may influence predator-prey dynamics directly or indirectly, contributing to existing community structure characteristics [31].

Predation has been recognized as an important factor in the evolution of adaptations, for example, chemical defenses and protective covering [26]. Predation, therefore, may select for certain species characteristics, impacting the ecology of a community.

5.2 Purple Sea Urchins and California Sheephead

Considering all the population data collected by the CINP Kelp Forest Monitoring program, we will focus this paper on modeling the predator-prey population dynamics between California sheephead and purple sea urchins. We will start by discussing the role of purple sea urchins in kelp forests, then moving on to California sheephead, and finally addressing their predator-prey relationship – and in Section 6.1 we will examine how that gives insight into model selection.

5.2.1 *Purple Sea Urchins*

Sea urchins live in environments that fluctuate between kelp forests and barrens, where the kelp forests are species rich – containing a high number of species – and the barrens are dominated by sea urchins [33]. The geographic range of purple sea urchins extends approximately 30° of latitude – from Alaska to Cedros Island, Mexico [13]. Within this range, adults in local populations are estimated to move no more than approximately tens or hundreds of meters throughout their lifetime [13]. Conversely, purple sea urchin larvae can be carried hundreds and

potentially thousands of kilometers from their origin point through feeding in plankton for about five weeks before settling [13].

Interestingly, sea urchin densities remain similar in both distinct forested and deforested states [33]. While sea urchin densities do not thrive in barrens, they also do not decline due to starvation [55]. Studies have inferred similar densities in forested and deforested areas exist because juvenile sea urchin post-settlement survival is higher in deforested areas than in forested kelp areas [37]. Since sea urchin densities are comparable between species rich kelp forests and barrens predominantly filled with urchins, sea urchins may be resilient toward differing living conditions – including food availability and the presence or absence of predators. Specifically, there may exist a particular minimum and maximum threshold at which sea urchins persist. The maximum threshold may act as a carrying capacity, which we will consider in some of our models.

Living in kelp forests, sea urchins remain nearly immobile where they feed on drift kelp, which are pieces of kelp litter released from kelp plants [33]. While sea urchins in kelp forests remain mostly stationary, storm events or El Niño events, can remove kelp, resulting in sea urchins needing to actively forage on young kelp and drift kelp from another place [33]. Feeding on young kelp, sea urchins contribute to facilitating an environment where kelp cannot establish successful forests [33].

Another factor influencing sea urchin density and ecological role is the spatial and temporal variation in sea urchin recruitment [33]. Peaks in recruitment that occur infrequently over time can lead to sudden increases in sea urchin abundance [33]. These quick surges of sea urchins have been observed to cause severe grazing, removing kelp faster than it can regrow, which leads to a barren dominated by sea urchins (Figure 5.2.1) [24] [33].

Historically, among the most important predators of urchins in California kelp forests are sheephead, spiny lobsters, abalone, and sea otters [24]. We will look more closely at the role California sheephead as predators of urchins in Section 5.2.3. In the 1950s, overfishing, exploitation, and ecological extinction of these particular predators led to the disappearance of California kelp forests [24]. The over exploitation of the sea urchin predators allowed the sea urchin population



Figure 5.2.1: Purple sea urchin barren, where after intense recruitment, purple sea urchins graze on remaining giant kelp holdfast in Carmel Bay ,California [Photo by M. Watanabe] [33] [55].

to increase without pressure from their predators, leading to the overgrazing and deforestation of kelp forests. In the 1970s and 1980s, however, fishing of the largest sea urchin species prompted a revival of established kelp forests [24].

Aside from the fishing of urchin predators, urchins have been observed to avoid predation through taking refuge [39] [15]. As urchins grow, they take refuge as they increase in size [39] [15]. Not only do they take refuge after reaching a size that can protect them, they also receive refuge from their surrounding environment, where they have been found to hide and take refuge in cobbles from predation [39]. The physical characteristics of their habitat, then, can be an asset to sea urchin vitality.

5.2.2 *California Sheephead*

The California sheephead species is in the Labridae genus [1]. While most fish in the same genus are small, not exploited reef fish, California sheephead can grow greater than 80 cm, and have historically experienced exploitation [1] [24]. Intense fishing of California sheephead affected their abundance and size distribution of sheephead in the 1940s and 50s [24] [46]. Their

range extends from Monterey Bay, California to Cabo San Lucas, Mexico, where they live in shallow temperate waters near the coast [1]. California sheephead are protogynous sequential hermaphrodites, meaning each individual changes from female to male during its life history [54].

California sheephead are generalist carnivores that feed on benthic invertebrates [19] [20] [28]. The specific taxa of benthic invertebrates California sheephead consume include echinoderms, mollusks, bryozoans, polychaetes, and crustaceans, where sea urchins are grouped into the echinoderm taxa [5] [20]. Previous studies demonstrated that California sheephead diet varies over substantial geographic scales, where their difference in diets between sites appeared to be described by site-specific prey availability [7] [20].

Not only do their diets alter depending on geographic location, California sheephead growth rates, natural mortality, size structure, and the timing of sex change and sexual maturity have been shown to vary with fishing impacts, temperature, and community conspecific densities [6] [21] [20]. A particular study indicated that California sheephead surrounding islands in California, Santa Catalina and San Nicolas, experienced changes in sex ratios and reductions in survivorship, average size of both sexes, and growth rates due to size-selective fishing compared with historical data [21].

While California sheephead have altered their characteristics due to a host of different variables, we will focus on their relationship with purple sea urchins, where the significance of urchins in California sheephead diet depends on geographical location and size [19]. Next, we will discuss their predator-prey relationship, before sorting through the data and constructing models.

5.2.3 California Sheephead and Purple Sea Urchin Predator-Prey Relationship

Since studies have shown sea urchin abundance remains relatively consistent between two extreme environments, kelp forests and barrens, we want to see if there is a relationship between a predator population, California sheephead, and an urchin population, purple sea urchin. To achieve this goal, we want to construct models that represent the current populations and predict future populations of both species. Modeling the purple sea urchin population with the Califor-

nia sheephead population can lend insight into whether or not California sheephead affect the persistence of the purple sea urchin population, and vice versa.

A study demonstrated that as the presence of the California sheephead increases, red sea urchins become less conspicuous [5]. This indicates that the presence of California sheephead, therefore, alters the behavior of urchins. More generally, this same study shows that sheephead can potentially regulate sea urchin population densities and distributions in their habitats [5]. Findings from another study suggest increased presence of California sheephead can cause heightened predation pressure on sea urchins, potentially leading to effects on kelp abundance [20]. Surveys in marine systems encompassing sheephead, urchins and fleshy macroalgae, which includes giant kelp, found negative relationships between sheephead and urchin abundance, and urchin and fleshy macroalgae abundance [19]. These reported negative relationships suggest that density-mediated indirect effects can occur where sheephead and other predator populations, and primary produces, such as kelp, experience positive growth, while the urchin populations experience negative growth [19].

As discussed, California sheephead are natural predators of purple sea urchins, we must now consider, then, ways purple sea urchins can escape predation from sheephead. Stated previously, urchins take refuge in size and have taken refuge by hiding in their environment [39] [15]. In kelp forests, then, kelp fronds may act as a means for purple sea urchins to hide in order to avoid predation by California sheephead and other predators. This creates an increasingly complex relationship between sheephead and urchins, and also urchins and kelp, as urchins feed on kelp and can potentially take refuge in the fronds.

Given the reported relationship between sheephead and sea urchins, we will explore the specific relationship between California sheephead and purple sea urchins by modelling their populations in Chapter 6. Before constructing our models, we must filter through data provided by the KFM Program which we will focus on next in Section 5.3.

5.3 Population Data

In this section we will discuss the protocol for measuring abundances of purple sea urchins and California sheephead. It is important to note that while there are 37 total sites, we will exclude sites 17, 18, 19 and 20, at San Clemente island because data were collected there for only two years [25]. We will then discuss and present which sites and years we included in our proceeding analysis to construct the models.

5.3.1 Purple Sea Urchins Methods

Purple sea urchins are among the most abundant species monitored by CINP in their monitoring program [25]. The KFM Program began collecting data on purple sea urchins in 1982 [25]. The number of sites used for data collection, however, have changed over time. In Table 5.3.1, we present the monitored sites and unmonitored sites from 1985 to 2011 for purple sea urchins.

Table 5.3.1: KFM Program monitored and unmonitored sites for purple sea urchins from 1982 to 2011.

Year	Monitored Sites	Unmonitored Sites
1982	1-4, 6-9, 11-15	5, 10, 16-37
1983-85	1-9, 11-15	10, 16-37
1986-00	1-16	17-37
2001-04	1-16, 21	17-20, 22-37
2005-11	1-16, 21-37	17-20

To measure purple sea urchin abundances, the KFM Program currently measures their density across 33 sites each year using a quadrat and random point contact method, also measuring size frequency [25]. We will not discuss size frequency calculations because data on size frequency were not collected until 2007, and in this paper we are considering only population abundance data, and not the size of the populations.

The quadrat method for measuring purple sea urchin abundance consists of 1 m quadrats placed along and parallel to the transect line [25]. The number of quadrats sampled at each site has changed over the years, where they used 30 in 1982, 40 from 1983-1984, 20 from 1985-

1995, and 12 from 1996 to present [25]. During this time there were small changes involved with entering data into the databases but these will not affect our overall analysis.

The random point contact method consists of sampling from a certain amount of points per quadrat at each site. The number of quadrats sampled as well as the number of points per quadrat have changed over time. In 1982 there were 25 quadrats with 20 points per quadrat, in 1983, 40 quadrats with 10 points per quadrat, in 1984, 10 quadrats with 50 points per quadrat, from 1985-1995, 25 quadrats with 40 points per quadrat, and from 1996- present, 15 quadrats with 40 points per quadrat [25]. Before 1996, the random point contact method placed quadrats at random points in an arranged form [25]. For the years after 1996, all sampling points contain randomly selected starting points [25]. At each quadrat, they sample a certain amount of points [25]. The total number of points sampled from annually, therefore, was 500 points in 1982, 400 points in 1983, 500 points in 1984, 1000 points from 1985-1995, and 600 points from 1996-present [25]. From 1985-1995, then, there were more points at which they measured abundance of sea urchins, which may affect the trends in urchin abundance. Using both techniques of measuring abundance, they consolidate their data to obtain one number for sea urchin density at each site during each year. While there were changes to their sampling method over time, for the purposes of our analysis we will consider all data to construct our models.

5.3.2 California Sheephead Methods

California sheephead data collection began in 1985 by the KFM Program [25]. Starting in 1985, they have continued to separate males and females in their count [25]. In 1996, they began collecting population data including and distinguishing the juvenile California sheephead [25]. In the models we will construct, however, we will exclude the juvenile data because the data-set provided to us by the KFM Program did not clarify if the data prior to 1996 contained juveniles [25]. Table 5.3.2 shows the monitored and unmonitored sites for California sheephead.

The KFM Program evaluates California sheephead abundance by calculating the relative abundance at each site using a roving diver fish count. They also use a visual transect sampling

Table 5.3.2: KFM Program monitored and unmonitored sites for California sheephead from 1985 to 2011.

Year	Monitored Sites	Unmonitored Sites
1985	1-6, 8-9, 11-15	7, 10, 16-37
1986-04	1-16	17-37
2005	1-16, 22-37	17-21
2006	1-16, 21-37	17-20
2007	1-16, 22-37	17-21
2008-11	1-16, 21-37	17-20

technique which as far as we can tell, however, is used for visualization and archival purposes and is not included in estimating relative abundances of California sheephead [25].

The roving diver fish count is a method for measuring abundance through the count of fish, where experienced divers, divers that can confidently identify and count all fish species in the Channel Islands, swim along and around the transect line for 30 minutes. The sampling area includes 10m on either side of the 100m transect line from the bottom to the surface [25].

5.3.3 Data Used for Analysis

Now considering both measurements of abundance for the purple sea urchin and California sheephead populations, first, for consistency purposes, we will eliminate any years and sites where there is not population data for both species.

Considering Table 5.3.1 and Table 5.3.2, we can see that while there is purple sea urchin data from 1982-1984, there is not data during those years for California sheephead populations. We will then, therefore, eliminate those years from our analysis. We also see that in 1985, data on California sheephead exclude sites 7, 10, and 16-37, while data on the purple sea urchin in 1985 exclude only sites 10, and 16-37. To achieve consistency across sites, we will remove data from site 7 for purple sea urchins. Following this same process of elimination to maintain uniformity, we will include the following years and sites in our study (Table 5.3.3).

Table 5.3.3: Included and excluded sites used to model purple sea urchin and California sheephead populations from 1985 to 2011.

Year	Included Sites	Excluded Sites
1985	1-6, 8-9, 11-15	7, 10, 16-37
1986-04	1-16	17-37
2005	1-16, 22-37	17-21
2006	1-16, 21-37	17-20
2007	1-16, 22-37	17-21
2008-11	1-16, 21-37	17-20

Now that we have established all of the sites and years we will use data for this study, we must then average the measures of abundance across all sites for each year to yield one value for each species for each year. We present these values in Table 5.3.4.

Table 5.3.4: Observed purple sea urchin average density and California sheephead average relative abundance from 1985 to 2011

Year	Purple sea urchin density	California sheephead relative abundance	Year	Purple sea urchin density	California sheephead relative abundance
1985	14.47	1.19	1999	22.34	1.16
1986	36.52	2.09	2000	46.75	1.08
1987	25.65	1.77	2001	27.77	0.69
1988	21.40	1.34	2002	19.91	0.66
1989	25.28	1.31	2003	8.00	0.38
1990	21.15	1.02	2004	12.14	0.44
1991	16.54	1.14	2005	16.42	0.41
1992	13.04	1.05	2006	17.69	0.71
1993	6.88	1.36	2007	16.71	0.41
1994	12.10	1.44	2008	22.25	0.41
1995	29.21	1.18	2009	25.58	0.51
1996	22.20	1.21	2010	23.22	1.02
1997	18.67	0.60	2011	33.61	0.84
1998	13.73	0.48			

To visualize these observed abundances for purple sea urchins and California sheephead, we can plot their population trajectories in Figure 5.3.1.

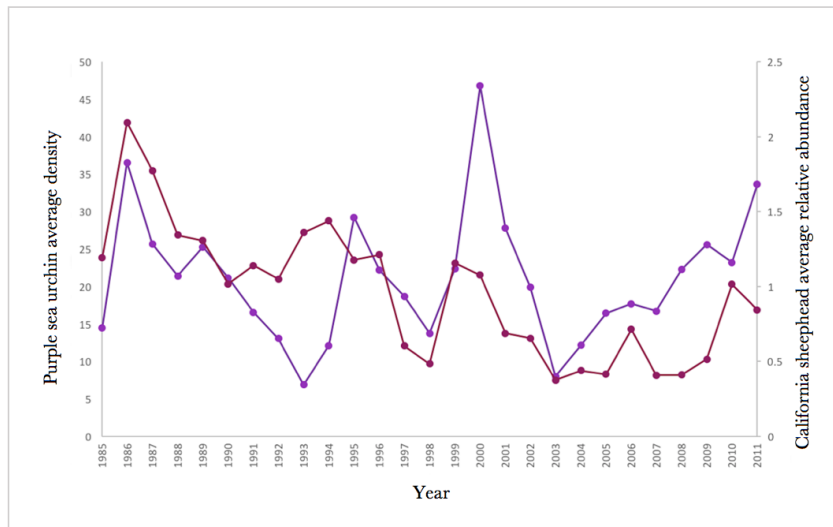


Figure 5.3.1: Observed purple sea urchin average density (purple) and California sheephead (maroon) average relative abundance in California kelp forests from 1985 to 2011. Data collected by CINP across 37 sites.

In Figure 5.3.1 we see the fluctuations in observed purple sea urchin average density and California sheephead average relative abundance over time. It is important to note the purple sea urchins and California sheephead correspond to two different scales represented by either y -axis. The purple sea urchin population seems to oscillate with no visible declining or increasing trend (Figure 5.3.1). The California sheephead population, however, seems to have a slight decreasing trend with peaks around the same time as the purple sea urchin population experiences peaks (Figure 5.3.1). This behavior where both species peak in abundance at similar times, we will try to explain using our models (Figure 5.3.1). There may, however, be outside environmental factors that are affecting both populations that we cannot pick up on in modeling their populations.

6

Applying known models to our data

6.1 Refining Models

To model the purple sea urchin and California sheephead populations, we start with the twelve possible models presented in Table 3.1.2. Out of these twelve models, we will eliminate half of them to keep a narrow focus and use only those that are consistent with other comparable studies and our own data.

Similar to other studies modeling predator-prey populations, we will use the two simplest models possible, incorporating a type I functional response with exponential growth and logistic growth – models 1 and 2 [28]. Since it has been observed that urchins take refuge from danger, including storm events or predation, we will include the models that incorporate a type I functional response with prey refuge – models 6 and 11 [39]. Finally, since sheephead are generalist carnivore consumers, we will include models that incorporate prey switching, which can be modeled using the type III functional response – models 4 and 9 [19] [28]. In order to analyze each of the chosen models as thoroughly as possible, we will not include models using a type II functional response nor models incorporating ratio-dependence – models 3, 5, 7, 8, 10, and 12 – to model purple sea urchin and California sheephead populations.

6.2 Fitting Models to our Data

To fit the models to our data, we first must set values to the constants in each model. We will start by defining the intrinsic growth rate, r , of purple sea urchins. There is no definitive study that determines growth rate of purple sea urchins. The intrinsic growth rate of red sea urchins, however, is estimated through studies. While again there is no known constant for the red sea urchin intrinsic growth rate, model predictions have estimated $r = 0.35$ [38]. We will use this value of intrinsic growth rate for purple sea urchins as a base value, and after constructing the models, we will try other values to see if there exist a better value from a range of 0.15 to 3.35.

Next, we will define the mortality rate, q , of California sheephead. First we will consider the survivorship of California sheephead, where survivorship is the proportion of individuals in a certain species surviving to each age class [1]. Previous studies demonstrate a range of values for survivorship for California sheephead from 0.577 to 0.745 across five different populations (Table 6.2.1) [6]. San Nicolas Island and Catalina Island are located in California, and Islas San

Table 6.2.1: California sheephead survivorship [6]

Population	Survivorship	Standard deviation
San Nicolas Island	0.745	0.02
Islas San Benitos	0.648	0.04
Cabo Thurloe	0.664	0.03
Isla Guadalupe	0.577	0.03
Catalina Island*	0.656	0.02
Isla Guadalupe*	0.630	0.02

Benitos, Cabo Thurloe, and Isla Guadalupe are located in Mexico. The data from populations with an asterisk (*) were taken from another study [6]. Along with these values for survivorship (Table 6.2.1), other studies have shown survivorship of the California sheephead estimated to be around 0.7 across two populations – Catalina Island and Guadalupe Island [1]. Using S to represent survivorship and q to be mortality rate:

$$S = e^{-q}. \tag{6.2.1}$$

Using the data from previous studies, we can calculate potential mortality rates given different values of survivorship using Equation 6.2.1. Solving for q using the lowest and highest survivorship values from the previous studies (Table 6.2.1) in Equation 6.2.1, values for the mortality rate range from approximately $q = 0.29$ to $q = 0.55$. Following other studies, we will use $q = 0.35$ as the standard natural mortality rate for our models, as it is between our approximate range [1]. We will also consider a greater range for q from $q = 0.05$ to $q = 0.95$ to find the best fit with the other parameters in the models.

Another constant we will set a baseline value for is the half-saturation constant. A study, which mined through data to provide an overview of the literature on half-saturation constants, reported half-saturation constant values between $h = 10^{-8}$ and $h = 10^{-4}$ for cold-blooded animals, where h represents the half-saturation constant [29]. The study reports that from their previous research, values for the half-saturation constant of cold-blooded carnivorous fish are within this range [29]. Units of h are in $[\text{kg}\cdot\text{km}^2, \text{kg}\cdot\text{l}^{-1}]$. As a starting value, therefore, we will let $h = 0.01$, and adjust in analysis of specific models.

To estimate the value of the constant number of purple sea urchins protected by refuges, we will start by setting $v = 0.01$, as the values for v in the study which supplied us with the expressions (Table 3.1.1) and tools for error estimation were $v = 5.6 \times 10^{-7}$ and $v = 1.1 \times 10^{-6}$ [34]. Using $v = 0.01$ as a starting constant, we will alter the value in each of the specific models.

We could not find available data regarding the carrying capacity of purple sea urchins. To find a possible starting value for carrying capacity, we will look to the observed data presented in Figure 6.2.1 and Table 5.3.4. In Figure 6.2.1, we can visualize the relationship between the purple sea urchin density and the California sheephead relative abundance. Carrying capacity, k , represents the maximum population that the environment can support [17]. To have a starting estimation of carrying capacity, we will use the purple sea urchin density at the black point, where their density is $V = 28.49$. This value at the black point represents a threshold – where purple sea urchin density increases and decreases before reaching the threshold, and declines after passing the threshold (Figure 6.2.1). This threshold then, may act as the carrying capacity

where the environment can no longer support a greater density of purple sea urchins. We will begin, therefore, using $k = 28.49$ as an initial condition for carrying capacity.

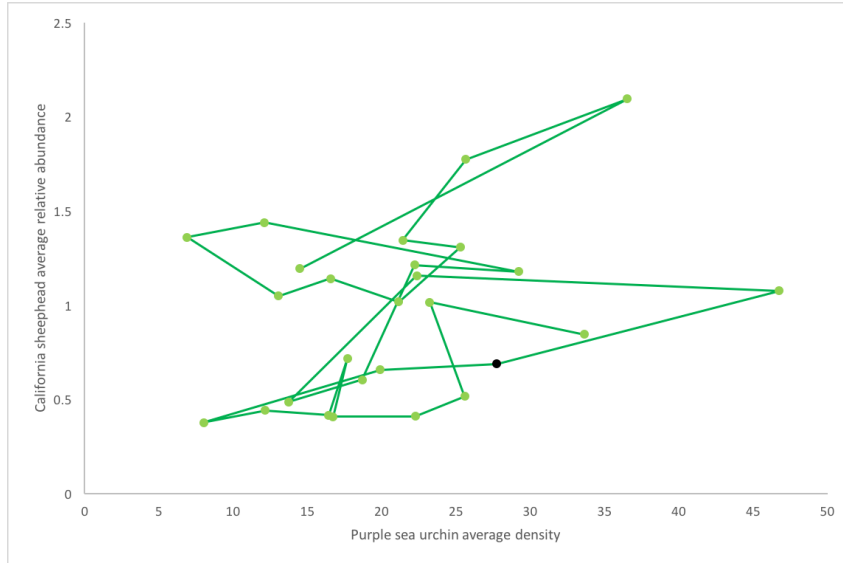


Figure 6.2.1: Relationship between purple sea urchin average density and California sheephead average relative abundance collected across 15 sites in California kelp forests from 1985 to 2011. Data collected by CINP. Black marker represents the data point with the greatest purple sea urchin density that leads to an increase in their density.

Using $r = 0.35$, $q = 0.35$, $h = 0.01$, $v = 0.01$ and $k = 28.49$ as our baseline conditions for the rate constants across all models where the constants are used, we must determine values for the other constants present in each model. Finding no published data or studies regarding the other constants in the six models specific to our two populations, we will rely on the provided population data and baseline values for r , q , h , v , and k . In doing so, we must calculate the value of the constants for each model individually – as the construction of each model may change the values of the parameters that will give us the best model for our two populations. For models containing β and α – models 1, 5, 7, and 11 – we begin by solving for those two constants using the baseline conditions of the other constants. For models including β and s – models 3 and 9 – we also start by solving for those two constants using the baseline constants.

We begin by presenting the values of each constant or parameter used in the first versions of each model in Table 6.2.2.

Table 6.2.2: Model constants for each model, $M_{i,1}$

Model	r	q	α	β	h	s	v	k
$M_{1,1}$	0.35	0.35	0.60	0.04				
$M_{2,1}$	0.35	0.35	0.32	0.05				28.49
$M_{4,1}$	0.35	0.35		0.04	0.01	14.63		
$M_{6,1}$	0.35	0.35	0.60	0.03			0.01	
$M_{9,1}$	0.35	0.35		0.05	0.01	5.80		28.49
$M_{11,1}$	0.35	0.35	0.32	0.05			0.01	28.49

To construct complete models, we must first find the values of the parameters without a determined value. We will do so by following the proceeding steps. First, calculate $\frac{dV}{dt}$ and $\frac{dP}{dt}$ from 1985, t_0 , to 1986, t_1 . Second, we will choose a model and will plug in those values for $\frac{dV}{dt}$ and $\frac{dP}{dt}$. Next we will substitute the observed values for V and P at t_0 , and the baseline parameters into the equations. Using the Solve function in Mathematica, we will find values to the two unknown parameters in the model at t_0 . We will repeat these steps for each time step through 2010. We cannot compute parameter values with 2011 as our initial time value because we do not have data for 2012, and therefore cannot calculate $\frac{dV}{dt}$ and $\frac{dP}{dt}$. We present values for $\frac{dV}{dt}$ and $\frac{dP}{dt}$ below in Table 6.2.3.

Table 6.2.3: Values for $\frac{dV}{dt}$ and $\frac{dP}{dt}$ from 1985 to 2011

Year	$\frac{dV}{dt}$	$\frac{dP}{dt}$	Year	$\frac{dV}{dt}$	$\frac{dP}{dt}$
1985-86	22.05	0.90	1998-99	8.61	0.68
1986-87	-10.87	-0.32	1999-00	24.41	-0.08
1987-88	-4.25	-0.43	2000-01	-18.98	-0.39
1988-89	3.88	-0.03	2001-02	-7.86	-0.03
1989-90	-4.13	-0.29	2002-03	-11.91	-0.28
1990-91	-4.61	0.12	2003-04	4.14	0.06
1991-92	-3.5	-0.09	2004-05	4.28	-0.03
1992-93	-6.16	0.31	2005-06	1.27	0.30
1993-94	5.22	0.08	2006-07	-0.98	-0.30
1994-95	17.11	1.18	2007-08	5.54	0.00
1995-96	-7.01	0.03	2008-09	3.33	0.10
1996-97	-3.5	-0.61	2009-10	-2.36	0.51
1997-98	-4.97	-0.12	2010-11	10.39	-0.18

After we have 26 values of our unknown constants, we will eliminate any values of the constants that are negative, and further eliminate the values that are outliers from the majority order of magnitude. In certain cases, we will include values for parameters that are near the very end or very beginning of the preceding or following order of magnitude, but will compensate by shifting the entire group so that it still only incorporates one order. For clarification, we will see an example of this when we consider $M_{6,1}$ on the following page. After removing the outliers, we will calculate the mean value for each of the parameters we are solving for, and use the mean values in the model. After these steps we will have a fully constructed model with all its parameters and create figures to visualize the model predictions. Finally, we will determine the type of equilibrium point following the procedure from Section 3.3 – but instead using actual values for the parameters in each model. We will follow this procedure for each of the six models.

To demonstrate this process of determining values for β , α , and s for each model, we will provide a sample calculation for how we find β and α in $M_{6,1}$.

Our first step is to calculate all 26 values of $\frac{dV}{dt}$ and $\frac{dP}{dt}$ (Table 6.2.3). Recall M_6 which is defined in Equation 3.2.2 where the set of differential equations is:

$$\begin{aligned}\frac{dV}{dt} &= rV - \alpha(V - v)P \\ \frac{dP}{dt} &= \beta\alpha(V - v)P - qP.\end{aligned}$$

Then, starting with 1985, we plug in $\frac{dV}{dt}$ and $\frac{dP}{dt}$ which we calculate using population data from 1985 subtracted from population data from 1986 (Table 6.2.3) so that we now have:

$$\begin{aligned}22.05 &= rV - \alpha(V - v)P \\ 0.90 &= \beta\alpha(V - v)P - qP.\end{aligned}\tag{6.2.2}$$

Then using the population data, we substitute $V = 14.47$ and $P = 1.19$ from 1985 (Table 5.3.4), along with the baseline values for the constants; $r = 0.35$, $q = 0.35$, and $v = 0.01$ into Equation 6.2.2:

$$\begin{aligned}22.05 &= 0.35(14.47) - \alpha(14.47 - 0.01)1.19 \\ 0.90 &= \beta\alpha(14.47 - 0.01)1.19 - 0.35(1.19).\end{aligned}\tag{6.2.3}$$

Solving for β and α we find that $\beta = -0.08$ and $\alpha = -0.99$. Now we repeat these steps until we have β and α for each time step, the results of which are shown in Table 6.2.4. To see these calculations in full, see Appendix A.

Table 6.2.4: Values for β and α in $M_{6,1}$

Year	β	α	Year	β	α
1985	-0.08	-0.99	1998	-0.22	-0.58
1986*	0.02	0.31	1999	-0.02	-0.64
1987*	0.01	0.29	2000	-0.0003	0.70
1988	0.12	0.13	2001*	0.01	0.92
1989*	0.01	0.39	2002	-0.003	1.44
1990*	0.04	0.56	2003	-0.14	-0.44
1991*	0.03	0.49	2004	-4.0	-0.01
1992	0.06	0.78	2005	0.10	0.67
1993	-0.20	-0.30	2006	-0.01	0.57
1994	-0.13	-0.74	2007	0.47	0.05
1995	0.03	0.50	2008*	0.05	0.49
1996	-0.02	0.42	2009*	0.06	0.87
1997*	0.01	1.03	2010	-0.08	-0.10

Now we have all 26 values for β and α (Table 6.2.4). Years with an asterisk (*) represent the parameters we use to calculate means. The process in which we eliminate the other years with values follows. Since all the parameters are defined in the models as positive rate constants, we must eliminate both the β and α values for any year which has a negative value for one of the parameters. We will also want to only keep the values for β and α that are not outliers within their own constant groups. Looking at Table 6.2.4, we see that the majority of the non-negative values for β are in the 10^{-2} order of magnitude. We will then, therefore, eliminate the values for β that are not in this magnitude and eliminate values for α in the corresponding years. For α we see that the majority of non-negative values are in the -1 order of magnitude (Table 6.2.4). The lowest α value in the -1 magnitude however, is $\alpha = 0.29$. We will then include values for α up to $\alpha = 1.28$, since the values do not span to the lowest values of the -1 order of magnitude.

Again, whatever values are eliminated due to the restrictions of α , we must also eliminate the corresponding β in the same year.

After eliminating the outliers, we now have a refined list of β and α for $M_{6.1}$, which are the values that correspond to the years marked with an asterisk (*) in Table 6.2.4. Finally, to obtain one value for each β and α we must calculate the mean values for each constant using the accepted refined values. Thus, we find:

$$\begin{aligned}\beta &= \text{Mean}[0.02, 0.01, 0.01, 0.04, 0.03, 0.06, 0.03, 0.01, 0.01, 0.05, 0.06, 0.03, 0.02] \approx 0.03 \\ \alpha &= \text{Mean}[0.31, 0.29, 0.39, 0.56, 0.49, 0.78, 0.50, 1.03, 0.92, 0.49, 0.87] \approx 0.60.\end{aligned}\tag{6.2.4}$$

Now we have values for all the parameters in $M_{6.1}$, which are as follows:

$$\begin{aligned}r &= 0.35 \\ q &= 0.35 \\ v &= 0.01 \\ \beta &= 0.03 \\ \alpha &= 0.60.\end{aligned}\tag{6.2.5}$$

We can construct $M_{6.1}$ substituting these parameters into the standard equation for M_6 (Equation 6.2.2) to get the following completed model:

$$\begin{aligned}\frac{dV}{dt} &= 0.35(V) - (0.60(V - 0.01)P) \\ \frac{dP}{dt} &= 0.03(0.06(V - 0.01)P) - 0.35(P).\end{aligned}\tag{6.2.6}$$

Using NDSolve in Mathematica, we can solve the differential equations and plot the prey, purple sea urchin, and predator, California sheephead, populations over time (Figure 6.2.2), where we display the specific estimated values for V and P in Table 6.2.5.

In Figure 6.2.2, we see that Model 6.1 predicts that both populations periodically oscillate over time, where between the time the purple sea urchins reach their maximum density and their minimum density, California sheephead will reach their maximum relative abundance (Figure 6.2.2). California sheephead will reach their minimum relative abundance while the purple sea urchin population increases from their minimum to maximum density. Model 6.1 then expects both populations to never go extinct and continue to oscillate periodically.

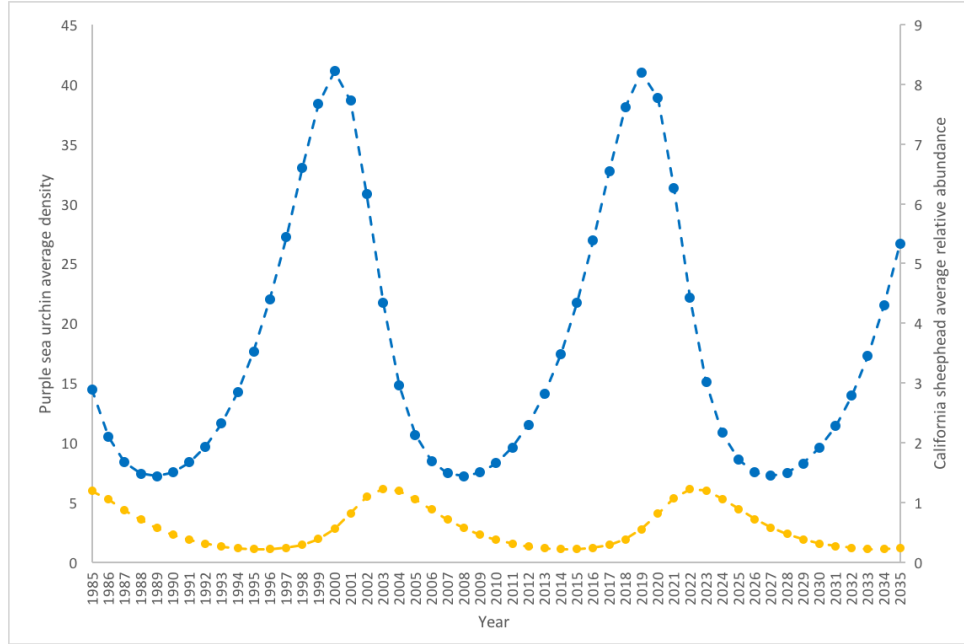


Figure 6.2.2: Model 6.1 predictions of density of purple sea urchin (blue) and relative abundance of California sheephead (yellow) from 1985 to 2035.

We can see more clearly the relationship between the purple sea urchin and California sheephead populations in Figure 6.2.3. In Figure 6.2.3, we see that the purple sea urchin and California sheephead populations plotted together, where each point on the figure represents a specific year, follow an elliptical shape over time – resembling Figure 2.1.3.

Now that we have graphical representations of the purple sea urchin and California sheephead populations over time as predicted by Model 6.1, let us now determine the type of equilibrium point for Model 6.1 with all its set parameters (Equation 6.2.6). Recall the Jacobian for M_6 (Equation 3.2.4) from Section 3.3 where:

$$J_{(V,P)} = \begin{bmatrix} r - P\alpha & -\alpha(V - v) \\ P\alpha\beta & -q + \alpha\beta(V - v) \end{bmatrix}.$$

Then, substituting the set rate constants into the $J_{(V,P)}$, we get:

$$J_{(V,P)} = \begin{bmatrix} 0.35 - 0.6P & -\alpha(V - 0.01) \\ 0.6(0.03)P & -0.35 + 0.6(0.03)(V - 0.01) \end{bmatrix}. \quad (6.2.7)$$

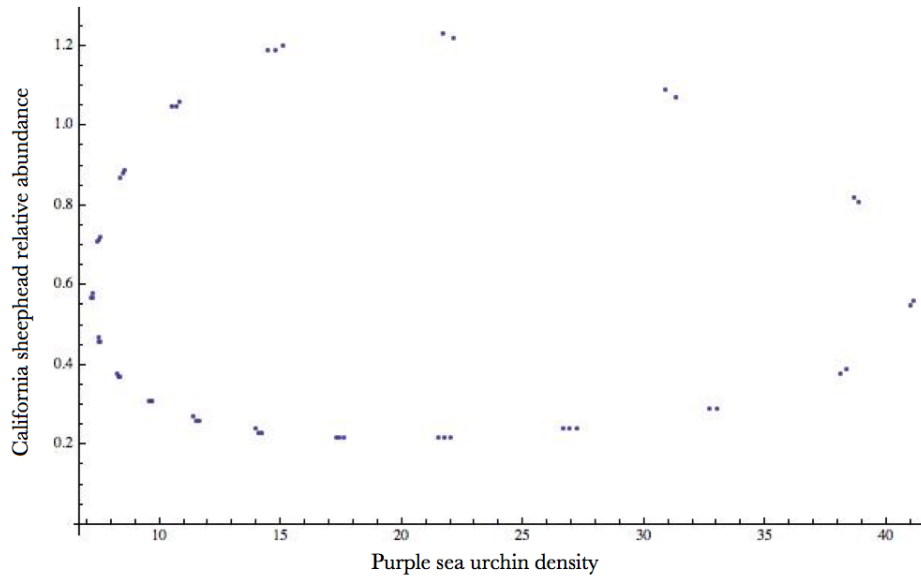


Figure 6.2.3: Model 6.1 predictions of the density of purple sea urchins and relative abundance of California sheephead. Each point represents both populations at a given time from 1985 to 2035.

Table 6.2.5: Model 6.1 predictions of the density of Purple sea urchins and relative abundance of California sheephead over time from 1985 to 2035.

Year	V_{est}	P_{est}	Year	V_{est}	P_{est}	Year	V_{est}	P_{est}	Year	V_{est}	P_{est}
1985	14.47	1.19	1998	33.01	0.29	2011	9.60	0.31	2024	10.83	1.06
1986	10.47	1.05	1999	38.35	0.39	2012	11.49	0.26	2025	8.56	0.89
1987	8.37	0.87	2000	41.09	0.56	2013	14.06	0.23	2026	7.51	0.72
1988	7.41	0.71	2001	38.63	0.82	2014	17.43	0.22	2027	7.22	0.58
1989	7.19	0.57	2002	30.85	1.09	2015	21.72	0.22	2028	7.49	0.47
1990	7.52	0.46	2003	21.69	1.23	2016	26.92	0.24	2029	8.26	0.38
1991	8.34	0.37	2004	14.78	1.19	2017	32.69	0.29	2030	9.54	0.31
1992	9.68	0.31	2005	10.66	1.05	2018	38.07	0.38	2031	11.40	0.27
1993	11.59	0.26	2006	8.47	0.88	2019	41.00	0.55	2032	13.93	0.24
1994	14.20	0.23	2007	7.46	0.71	2020	38.86	0.81	2033	17.26	0.22
1995	17.63	0.22	2008	7.20	0.57	2021	31.30	1.07	2034	21.50	0.22
1996	21.97	0.22	2009	7.50	0.46	2022	22.12	1.22	2035	26.65	0.24
1997	27.21	0.24	2010	8.30	0.37	2023	15.08	1.20			

Solving for the equilibrium point of Equation 6.2.6, we find that $V^* = 19.45$ and $P^* = 0.58$.

Plugging in the equilibrium point to Equation 6.2.7, we find:

$$J_{(V^*,P^*)} = \begin{bmatrix} 0.002 & -11.664 \\ 0.01044 & -0.00008 \end{bmatrix}, \quad (6.2.8)$$

where

$$\det J_{(V,P)} = 0.12 \quad (6.2.9)$$

$$\text{tr } J_{(V,P)} = 0.00192$$

and

$$\lambda_1 = 0.0096 + 0.348957i \quad (6.2.10)$$

$$\lambda_2 = 0.0096 - 0.348957i.$$

Given the eigenvalues, determinant and trace, we can determine that the equilibrium is a spiral source. Referencing Section 3.2, we know that the equilibrium of Model 6.1 is a spiral source because $0.12 > 0.00192/4$ and $0.00192 > 0$ [51]. Figure 6.2.3, however, demonstrates that the solutions follow a closed loop in the short term, from 1985-2035. This may be because 0.00192 is close to zero, therefore, the solutions over the long run spiral in toward the equilibrium point but do so only slightly at each time step.

After constructing $M_{1.1}, M_{2.1}, M_{4.1}, M_{6.1}, M_{9.1}$ and $M_{11.1}$, we construct second versions of each model, $M_{1.2}, M_{2.2}, M_{4.2}, M_{6.2}, M_{9.2}$ and $M_{11.2}$ using the initial parameter values $r = 3.35$, $q = 0.85$, $h = 0.01$, $v = 0.01$ and $k = 28.49$. Running through the same process as shown with $M_{6.1}$, the six new constructed models have the parameter values displayed in Table 6.2.6.

Table 6.2.6: Model constants for each model, $M_{i,2}$

Model	r	q	α	β	h	s	v	k
$M_{1.2}$	3.35	0.85	4.24	0.02				
$M_{2.2}$	3.35	0.85	2.26	0.04				28.49
$M_{4.2}$	3.35	0.85		0.01	0.01	64.94		
$M_{6.2}$	3.35	0.85	4.19	0.02			0.01	
$M_{9.2}$	3.35	0.85		0.03	0.01	32.84		28.49
$M_{11.2}$	3.35	0.85	2.39	0.03			0.01	28.49

After creating two versions of each model, we use the Manipulate function in Mathematica to try to find the values for each constant that best represents the observed data from Table

5.3.4 which is visualized in Figure 5.3.1. After using Manipulate, we have more versions of each model, whose parameters are displayed in Table 6.2.7.

Table 6.2.7: Model constants for each model, $M_{i,i}$

Model	r	q	α	β	h	s	v	k
$M_{1.3}$	0.79	0.47	0.40	0.05				
$M_{2.3}$	0.46	0.59	0.96	0.027				150
$M_{4.3}$	0.35	0.35		0.06	10.5	14.63		
$M_{4.4}$	0.48	0.49		0.054	12.9	18.1		
$M_{4.5}$	0.78	0.36		0.053	14.99	13.80		
$M_{4.6}$	0.44	0.50		0.054	12.9	18.1		
$M_{4.7}$	0.51	0.47		0.052	12.9	18.1		
$M_{6.3}$	0.50	0.99	0.51	0.07			0.01	
$M_{6.4}$	0.59	0.91	0.51	0.07			0.01	
$M_{9.3}$	0.95	0.67		0.08	14.99	13.8		147.5
$M_{11.3}$	3.35	0.45	0.42	0.05			0.01	28.49
$M_{11.4}$	0.85	0.39	0.33	0.067			0.01	500
$M_{11.5}$	0.82	0.39	0.33	0.06			0.01	2500

Now to calculate the model of best fit, we must the compute error estimation for each model. To do so, our first step is to determine which objective function, F , is most appropriate. As stated in Section 3.3, we have four possible objective functions. Running all four possibilities for F on each model, we use each of our values for F and calculate ET to compute R_i^2 for each model (Equation 3.3.1). The objective function which outputs the most comprehensive R^2 value, we will use for our complete analysis.

6.3 Error Estimation

Before calculating the model of best fit, let's first recall the necessary functions defined in Section 3.3 and Equation 3.3.1, where:

$$F = \begin{cases} F_{of_1} = \sum_{n=1}^n [(V_{obs_i} - V_{est_i})^2 + (P_{obs_i} - P_{est_i})^2], \\ F_{of_2} = \sum_{n=1}^n \left[\left(\frac{V_{obs_i} - V_{est_i}}{V_{obs_i}} \right)^2 + \left(\frac{P_{obs_i} - P_{est_i}}{P_{obs_i}} \right)^2 \right], \\ F_{of_3} = \sum_{n=1}^n F_i = \sum_{n=1}^n \{ [\omega_v (V_{obs_i} - V_{est_i})]^2 + [\omega_P (P_{obs_i} - P_{est_i})]^2 \} \\ \frac{\omega_v}{\omega_P} = \frac{\sigma_P}{\sigma_v} \Rightarrow \omega_P = 1 \therefore \omega_v = \frac{\sigma_P}{\sigma_v}, \\ F_{of_4} = \sum_{n=1}^n \left[\frac{(V_{obs_i} - V_{est_i})^2}{V_{obs_i}} + \frac{(P_{obs_i} - P_{est_i})^2}{P_{obs_i}} \right], \end{cases}$$

and

$$ET = \sum_{n=1}^n \{ [\omega_v (V_{obs_i} - \bar{V})]^2 + [\omega_P (P_{obs_i} - \bar{P})]^2 \}$$

$$R^2 = \frac{ET - F}{ET}.$$

Then, let us calculate the total variation, ET , of our data. The total variation is the same across all models because it is written in terms of the observed data. Using the observed data we calculate the means and find:

$$\bar{V} = 21.08 \tag{6.3.1}$$

$$\bar{P} = 0.96.$$

We present values for V_{obs_i} and P_{obs_i} in Table 5.3.4. Calculating ET using unweighted total variation, we use:

$$\omega_v = 1 \tag{6.3.2}$$

$$\omega_P = 1$$

where we now can solve for ET . Using our values for \bar{V} , V_{obs_i} , P_{obs_i} , \bar{P} , ω_v , and ω_P , we get:

$$ET = 1856.62 \tag{6.3.3}$$

We will now show an example of calculating the error estimation for $M_{6.1}$. We have four possible objective functions from Section 3.3. Calculating F_{of_i} for $M_{6.1}$ using the Sum function in Mathematica, we find:

$$\begin{aligned} F_{of_1} &= 4656.0 \\ F_{of_2} &= 30.553 \\ F_{of_3} &= 121.13 \\ F_{of_4} &= 226.40. \end{aligned} \tag{6.3.4}$$

Next, substituting each of the values for F_{of_i} and our value for ET into Equation 3.3.1 for R^2 we can calculate four different values for R_i^2 , where:

$$\begin{aligned} R_1^2 &= -1.509 \\ R_2^2 &= 0.9835 \\ R_3^2 &= -64.24 \\ R_4^2 &= 0.8781. \end{aligned} \tag{6.3.5}$$

Considering each R_i^2 value, we can eliminate F_{of_1} and F_{of_3} as possible objective functions because they yield negative R_i^2 values. R_i^2 measures the amount of variation explained by the model, where its values are between 0 and 1, such that 0 demonstrates the model explains no variation and 1 indicates the model explains 100 percent of the variation [34].

Then we have F_{of_2} and F_{of_4} as possible objective functions. Using objective function F_{of_2} to solve for R_2^2 , predicts that Model 6.1 explains 98.35 percent of the variation. Using objective function F_{of_4} to solve for R_4^2 , predicts that Model 6.1 explains 87.81 percent of the variation. The second objective function, then, considers Model 6.1 to fit the data better than the fourth objective function suggests.

To determine how much variation $M_{6.1}$ explains, we must determine which objective function to use in our final analysis. If we cannot confidently choose an objective function, between F_{of_2} and F_{of_4} , to use in calculating error estimation, we will compare R_2^2 and R_4^2 values obtained using each objective function for all models, $M_{i,i}$, and then draw conclusions. To do so, we will calculate F_{of_2} and R_2^2 , and F_{of_4} and R_4^2 for each model, $M_{i,i}$. The results of these calculations are presented in Table 6.3.1.

It is important to note that using the estimated population data from Model 4.2 yields objective functions significantly greater than all other models, also having negative R_i^2 values using both objective functions. Looking at Figure 6.3.1, we can see that the purple sea urchin and California sheephead populations in Model 4.2 do not represent the observed data (Figure 5.3.1), where the values are different by orders of magnitude. The other two potential objective functions, F_{of_1} and F_{of_3} generate negative R_i^2 for all models. We will continue to use, therefore, the

Table 6.3.1: Values for objective functions 1 and 2, and their corresponding R_i^2 values. R_2^2 values with an asterisk (*) represent the two models of best fit predicted by using the second objective function, and R_4^2 values with an star (*) represent the two models of best fit predicted by using the fourth objective function.

Model	F_{of_i}	R_i^2	Model	F_{of_i}	R_i^2
$M_{1.1}$	$F_{of_2} = 27.70$	$R_2^2 = 0.9851$	$M_{6.1}$	$F_{of_2} = 30.55$	$R_2^2 = 0.9835$
	$F_{of_4} = 213.0$	$R_4^2 = 0.8853$		$F_{of_4} = 226.4$	$R_4^2 = 0.8781$
$M_{1.2}$	$F_{of_2} = 23.33$	$R_2^2 = 0.9874$	$M_{6.2}$	$F_{of_2} = 22.74$	$R_2^2 = 0.9878$
	$F_{of_4} = 259.8$	$R_4^2 = 0.8601$		$F_{of_4} = 247.8$	$R_4^2 = 0.8665$
$M_{1.3}$	$F_{of_2} = 129.0$	$R_2^2 = 0.9305$	$M_{6.3}$	$F_{of_2} = 44.60$	$R_2^2 = 0.9760$
	$F_{of_4} = 219.9$	$R_4^2 = 0.8815$		$F_{of_4} = 307.5$	$R_4^2 = 0.8345$
$M_{2.1}$	$F_{of_2} = 18.78$	$R_2^2 = 0.9899$	$M_{6.4}$	$F_{of_2} = 40.94$	$R_2^2 = 0.9779$
	$F_{of_4} = 132.2$	$R_4^2 = 0.9288^*$		$F_{of_4} = 220.7$	$R_4^2 = 0.8811$
$M_{2.2}$	$F_{of_2} = 21.71$	$R_2^2 = 0.9883$	$M_{9.1}$	$F_{of_2} = 44.80$	$R_2^2 = 0.9759$
	$F_{of_4} = 207.4$	$R_4^2 = 0.8883$		$F_{of_4} = 541.1$	$R_4^2 = 0.7086$
$M_{2.3}$	$F_{of_2} = 28.73$	$R_2^2 = 0.9845$	$M_{9.2}$	$F_{of_2} = 46.50$	$R_2^2 = 0.9750$
	$F_{of_4} = 302.7$	$R_4^2 = 0.8369$		$F_{of_4} = 379.2$	$R_4^2 = 0.7957$
$M_{4.1}$	$F_{of_2} = 47.54$	$R_2^2 = 0.9744$	$M_{9.3}$	$F_{of_2} = 157.4$	$R_2^2 = 0.9152$
	$F_{of_4} = 570.6$	$R_4^2 = 0.6926$		$F_{of_4} = 227.6$	$R_4^2 = 0.8774$
$M_{4.2}$	$F_{of_2} = 1.588 \times 10^{40}$	$R_2^2 = -8.553 \times 10^{36}$	$M_{11.1}$	$F_{of_2} = 18.79$	$R_2^2 = 0.9899$
	$F_{of_4} = 5.333 \times 10^{41}$	$R_4^2 = -2.872 \times 10^{38}$		$F_{of_4} = 132.2$	$R_4^2 = 0.9288^*$
$M_{4.3}$	$F_{of_2} = 18.91$	$R_2^2 = 0.9898$	$M_{11.2}$	$F_{of_2} = 30.98$	$R_2^2 = 0.9833$
	$F_{of_4} = 252.1$	$R_4^2 = 0.8642$		$F_{of_4} = 300.9$	$R_4^2 = 0.8379$
$M_{4.4}$	$F_{of_2} = 12.36$	$R_2^2 = 0.9933^*$	$M_{11.3}$	$F_{of_2} = 111.2$	$R_2^2 = 0.9401$
	$F_{of_4} = 149.5$	$R_4^2 = 0.9195$		$F_{of_4} = 172.8$	$R_4^2 = 0.9069$
$M_{4.5}$	$F_{of_2} = 143.0$	$R_2^2 = 0.9230$	$M_{11.4}$	$F_{of_2} = 240.1$	$R_2^2 = 0.8707$
	$F_{of_4} = 189.7$	$R_4^2 = 0.8978$		$F_{of_4} = 215.1$	$R_4^2 = 0.8841$
$M_{4.6}$	$F_{of_2} = 13.18$	$R_2^2 = 0.9929$	$M_{11.5}$	$F_{of_2} = 281.2$	$R_2^2 = 0.8485$
	$F_{of_4} = 153.7$	$R_4^2 = 0.9172$		$F_{of_4} = 276.7$	$R_4^2 = 0.8510$
$M_{4.7}$	$F_{of_2} = 12.65$	$R_2^2 = 0.9932^*$			
	$F_{of_4} = 148.9$	$R_4^2 = 0.9198$			

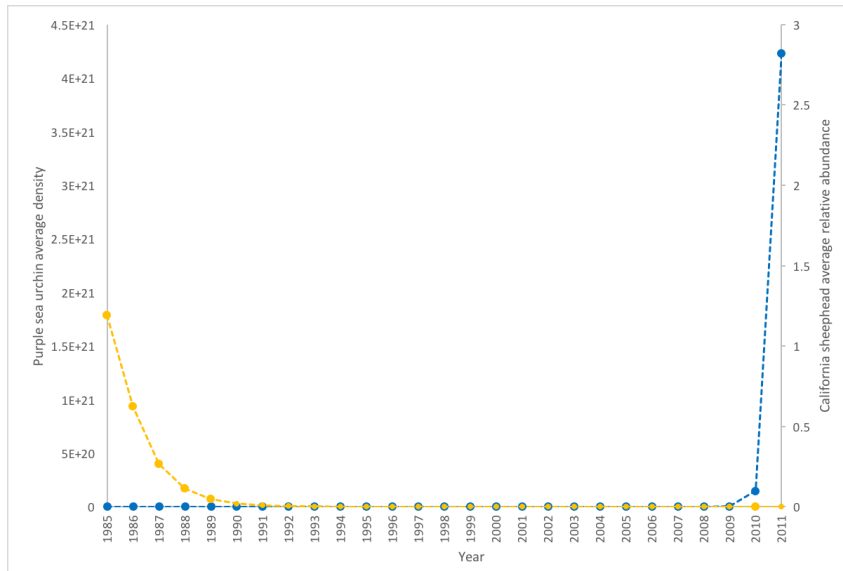
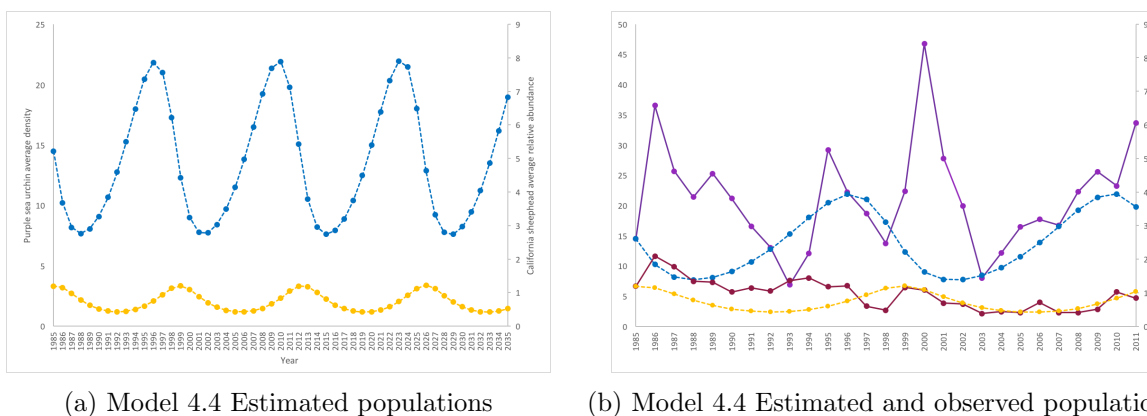


Figure 6.3.1: Model 4.2 predictions of purple sea urchin (blue) and California sheephead (yellow) populations from 1985 to 2011.

second and fourth objective functions for further analysis, where we can not, however explain the error of Model 4.2.

After calculating R_i^2 using the second and fourth objective functions we find that the second objective function determines that Model 4.4 (Figure 6.3.2) is the model that best fits the purple sea urchin and California sheephead data, where $R_2^2 = 0.9933$ (Table 6.3.1). The second objective

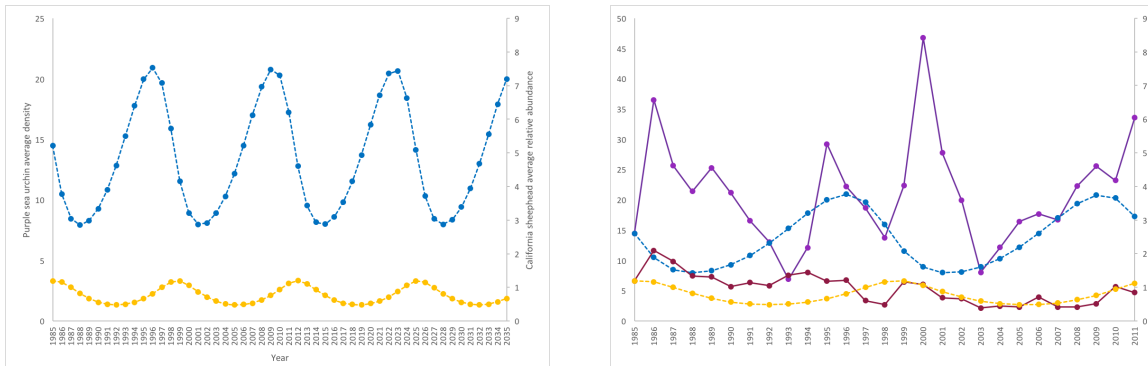


(a) Model 4.4 Estimated populations

(b) Model 4.4 Estimated and observed populations

Figure 6.3.2: Observed (solid) and estimated (dashed) purple sea urchin and California sheephead populations over time. All axes are consistent with the axes labels in plot a. Plot a depicts the change in population of purple sea urchin (blue) and California sheephead (yellow) from 1985 to 2035 as predicted by Model 4.4. Plot b shows the results of Model 4.4 with the observed purple sea urchin (purple) and California sheephead (maroon) populations from 1985 to 2011.

function also predicts that Model 4.7 (Figure 6.3.3) is the second most accurate model where $R_2^2 = 0.9932$.

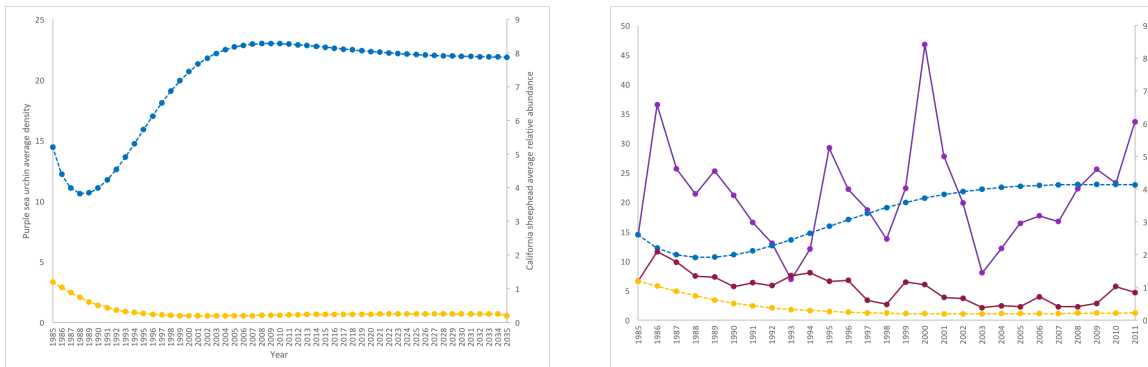


(a) Model 4.7 Estimated populations

(b) Model 4.7 Estimated and observed populations

Figure 6.3.3: Observed (solid) and estimated (dashed) purple sea urchin and California sheephead populations over time. All axes are consistent with the axes labels in plot a. Plot a depicts the change in population of purple sea urchin (blue) and California sheephead (yellow) from 1985 to 2035 as predicted Model 4.7. Plot b shows the results of Model 4.7 with the observed purple sea urchin (purple) and California sheephead (maroon) populations from 1985 to 2011.

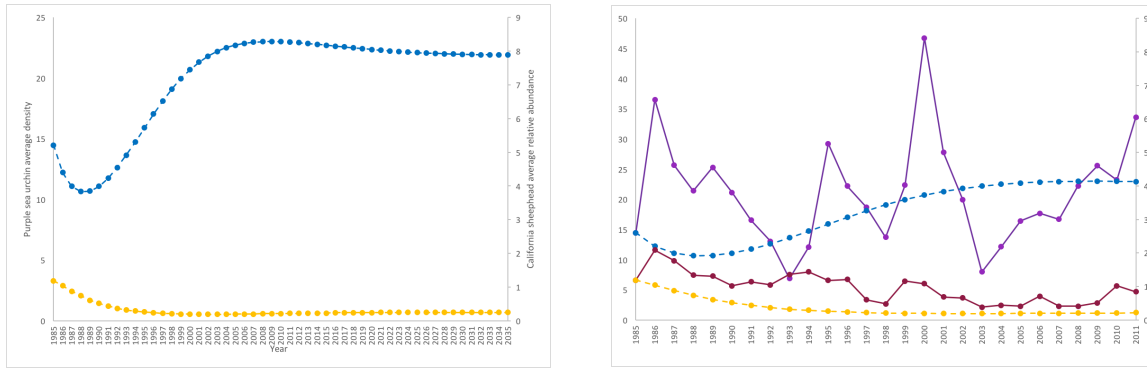
The fourth objective functions suggests that Model 2.1 (Figure 6.3.4) and Model 11.1 (Figure 6.3.5) explain the most variation of the data where $R_4^2 = 0.9288$ for both models (Table 6.3.1). Using the fourth objective function in our calculations for R_i^2 , then, yields Models 2.1 and 11.1 as the models of best fit.



(a) Model 2.1 Estimated populations

(b) Model 2.1 Estimated and observed populations

Figure 6.3.4: Observed (solid) and estimated (dashed) purple sea urchin and California sheephead populations over time. All axes are consistent with the axes labels in plot a. Plot a depicts the change in population of purple sea urchin (blue) and California sheephead (yellow) from 1985 to 2035 as predicted Model 2.1. Plot b shows the results of Model 2.1 with the observed purple sea urchin (purple) and California sheephead (maroon) populations from 1985 to 2011.



(a) Model 11.1 Estimated populations

(b) Model 11.1 Estimated and observed populations

Figure 6.3.5: Observed (solid) and estimated (dashed) purple sea urchin and California sheephead populations over time. All axes are consistent with the axes labels in plot a. Plot a depicts the change in population of purple sea urchin (blue) and California sheephead (yellow) from 1985 to 2035 as predicted Model 11.1. Plot b shows the results of Model 11.1 with the observed purple sea urchin (purple) and California sheephead (maroon) populations from 1985 to 2011.

Now that we have determined the two models for each objective functions that explain most the variation in our data, we must consider which objective function produces the most accurate R_i^2 values, and draw conclusions based on our findings.

7

Conclusions

7.1 Error Estimation Discussion

As we found in Chapter 6, Models 4.4 (Figure 6.3.2) and 4.7 (Figure 6.3.3), and Models 2.1 (Figure 6.3.4) and 11.1 (Figure 6.3.5) fit the purple sea urchin and California sheephead population best according to the second and fourth objective functions, respectively.

Let us first consider the results from the second objective function. Depicted in Figure 6.3.2 and Figure 6.3.3, the estimated data from both Model 4.4 and Model 4.7 look almost identical, as the data follow the same trend. For both models, it appears that the variation between the estimated and observed purple sea urchin average densities is greater than the variation between the estimated and observed average relative abundance of California sheephead (Figure 6.3.2b, Figure 6.3.3b). For both models after 1998, the variation between the estimated and observed population values for California sheephead decreases (Figure 6.3.2b, Figure 6.3.3b). Model 4.4 and Model 4.7 both predict that the populations will oscillate over time (Figure 6.3.2a, Figure 6.3.3a). We can also depict the cycles of purple sea urchin and California sheephead populations in Figure 7.1.1.

Determining the positive non-zero equilibrium points of Model 4.4, we find that $V^* = 12.93$ and $P^* = 0.68$, where E^* is defined as a spiral source. For Model 4.7, we have an equilibrium

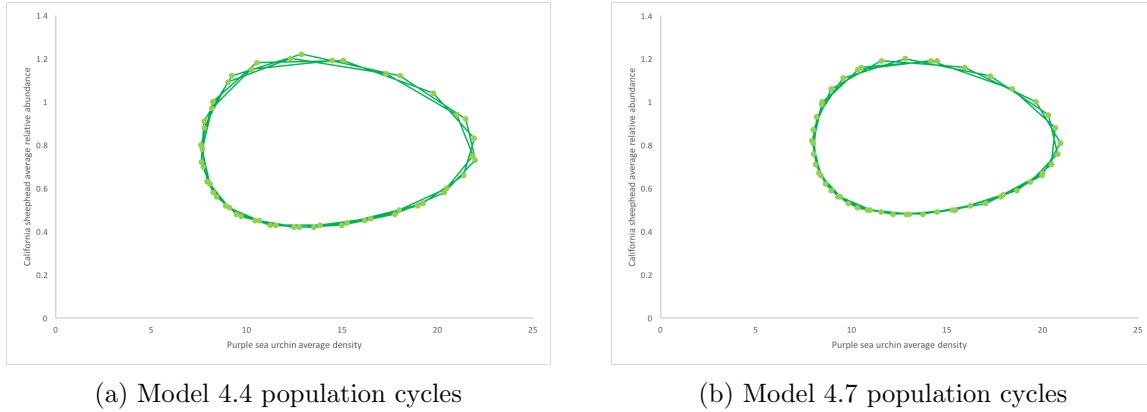


Figure 7.1.1: Purple sea urchin and California sheephead population cycles predicted by (a) Model 4.4 and (b) Model 4.7. Each point represents both population abundances at a given time from 1985 to 2035.

point where $V^* = 12.88$ and $P^* = 0.73$, where the solutions follow a spiral sink. See Appendix B for detailed work demonstrating how we arrived at these equilibrium points.

The fourth objective function states that Model 2.1 and Model 11.1 explain the same amount of variation and are the best models. Again, the variation between estimated and observed California sheephead populations seems to be less than the variation for purple sea urchins (Figure 6.3.4b, Figure 6.3.5b). The population trajectories for both models show that the purple sea urchin and California sheephead populations level out over time (Figure 6.3.4a, Figure 6.3.5a). Plotting their population cycles, we can see the relationship between the purple sea urchin and

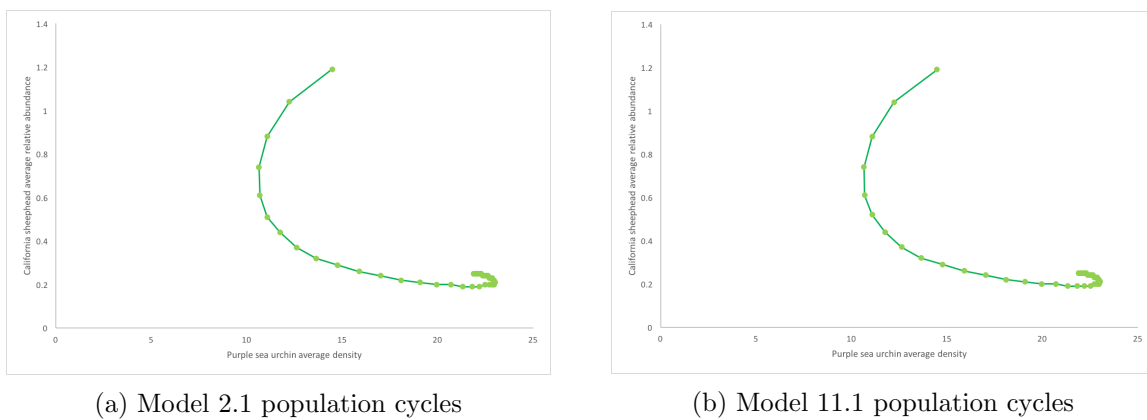


Figure 7.1.2: Purple sea urchin and California sheephead population cycles predicted by (a) Model 2.1 and (b) Model 11.1. Each point represents both population abundances at a given time from 1985 to 2035.

California sheephead populations (Figure 7.1.2). Instead of seeing periodic cycles, as we did examining Model 4.4 and Model 4.7, we see that both populations begin to decline, leading to an increase in purple sea urchin average density, and finally resulting in a slight increase in sheephead and decrease in purple sea urchin average density (Figure 7.1.2).

Determining the positive non-zero equilibrium points of Model 2.1, we find that there are two equilibrium points, one containing a negative value for P^* and the other containing a zero value for P^* . There are, therefore, no positive non-zero equilibrium points for Model 2.1. Since there cannot be negative of a population, but it is possible for a population to reach zero, we will consider the equilibrium point where $V^* = 28.49$ and $P^* = 0$, such that E^* is defined as a source. For Model 11.1, we have an equilibrium point where $V^* = 12.89$ and $P^* = 0.25$, where the solutions follow a spiral sink. Again, Appendix B contains the work for determining equilibrium points, including trace, determinants, and eigenvalues.

To compare the two objective functions let us rank the best predicted models using both objective functions (Table 7.1.1). Using both objective functions to calculate the models of best

Table 7.1.1: Six best models as predicted using the second and fourth functional responses to calculate R_i^2 .

Rank	Model	R_2^2	Rank	Model	R_4^2
1	$M_{4.4}$	0.9933	1	$M_{2.1}$	0.9288
2	$M_{4.7}$	0.9932	1	$M_{11.1}$	0.9288
3	$M_{4.6}$	0.9929	3	$M_{4.7}$	0.9198
4	$M_{2.1}$	0.9899	4	$M_{4.4}$	0.9195
4	$M_{11.1}$	0.9899	5	$M_{4.6}$	0.9172
6	$M_{4.3}$	0.9898	6	$M_{11.3}$	0.9069

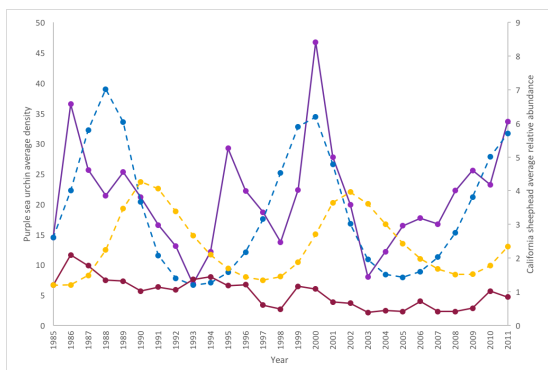
fit, we find that the best six models are consistent using both objective functions (Table 7.1.1). While the same six models are determined as the best fit using either objective function to calculate R_i^2 , they are ranked differently according to which objective function we use (Table 7.1.1). In this case, the objective function matters less in determining which models best fit the data, but matters more in determining how well each model describes total variation of the data. For this reason, we will focus on the range of R_i^2 values. We will look, then, at the six models

that explained the least amount of variation in the data according to either objective function (Table 7.1.2).

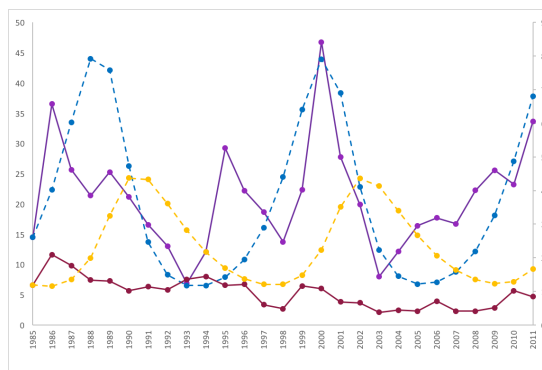
Table 7.1.2: Six models of least fit as predicted using the second and fourth functional responses to calculate R_i^2 .

Rank	Model	R_2^2	Rank	Model	R_4^2
1	$M_{11.5}$	0.8485	1	$M_{4.1}$	0.6926
2	$M_{11.4}$	0.8707	2	$M_{9.1}$	0.7086
3	$M_{9.3}$	0.9152	3	$M_{9.2}$	0.7957
4	$M_{4.5}$	0.9230	4	$M_{6.3}$	0.8345
5	$M_{1.3}$	0.9305	5	$M_{2.3}$	0.8369
6	$M_{4.1}$	0.9744	6	$M_{11.2}$	0.8379

Unlike the overlaps we found in determining the best models using either objective function, the six models of least fit corresponding to either objective function have only one overlap, Model 4.1 (Table 7.1.2). There is a more apparent effect of which objective function is best for analysis when looking at worst models determined by R_i^2 . Figure 7.1.3 and Figure 7.1.4 depict the estimated population values for Model 11.5 and 11.4, and Model 4.1 and Model 9.1, respectively.



(a) Model 11.4



(b) Model 11.5

Figure 7.1.3: Observed (solid) and estimated (dashed) purple sea urchin and California sheephead populations over time. All axes are consistent with the axes labels in plot a. Plot a depicts the estimated purple sea urchin (blue) and California sheephead (yellow) from 1985 to 2035 as predicted Model 11.4 with the observed purple sea urchin (purple) and California sheephead (maroon) populations from 1985 to 2011. Plot b shows the estimated purple sea urchin and California sheephead from 1985 to 2035 as predicted Model 11.5 with the observed populations from 1985 to 2011.

Looking at Figure 7.1.3, we see that for both models, the estimated purple sea urchin population appears to follow the trend of the observed population values. The more apparent variation in these models is between the estimated and observed California sheephead population. After 1987, the estimated California sheephead population is always greater than the observed, and oscillates to form clear peaks and troughs which the estimated population doesn't follow (Figure 7.1.3).

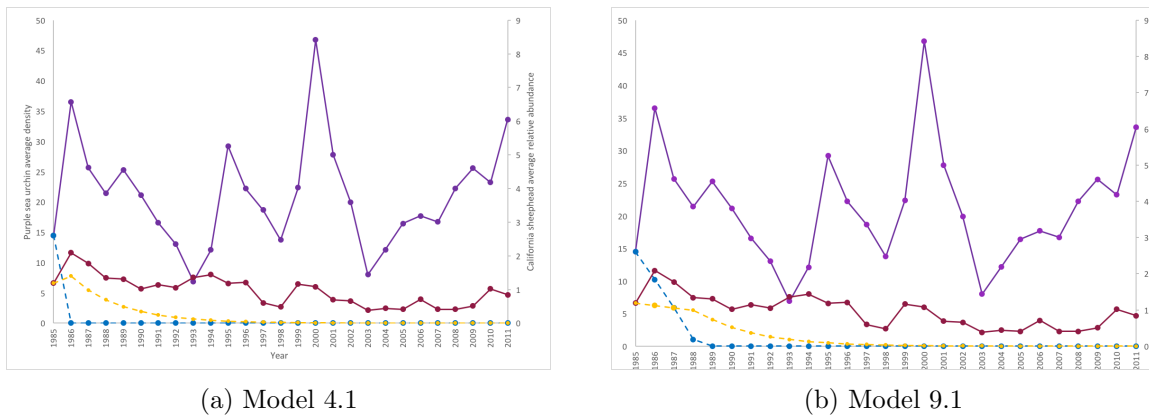


Figure 7.1.4: Observed (solid) and estimated (dashed) purple sea urchin and California sheephead populations over time. All axes are consistent with the axes labels in plot a. Plot a depicts the estimated purple sea urchin (blue) and California sheephead (yellow) from 1985 to 2035 as predicted Model 4.1 with the observed purple sea urchin (purple) and California sheephead (maroon) populations from 1985 to 2011. Plot b shows the estimated purple sea urchin and California sheephead from 1985 to 2035 as predicted Model 9.1 with the observed populations from 1985 to 2011.

In Figure 7.1.4, we see the results of Model 4.1 in plot a and the results of Model 9.1 in plot b. Both models predict that the purple sea urchin and the California sheephead population decline as they approach zero (Figure 7.1.4). The variation, therefore, is evident across both populations in either model (Figure 7.1.4).

Now that we have graphically presented the two models of least fit produced by calculating R_i^2 using objective functions 2 and 4, we can see that both objective functions do not agree in calculating the fitness of each model – which we did not see, necessarily, when considering the models of best fit. By looking at the best and least fit models corresponding to the second and

fourth objective functions, we can not determine which objective function to use to calculate R_i^2 to find the models that best fit our data.

Given our findings, however, Model 4.4 determined using the second objective function, and Model 2.1 and Model 11.1 determined using the fourth objective function, are the models of best fit. Model 4.4 incorporates exponential growth and a type III functional response and is constructed as follows:

$$\begin{aligned}\frac{dV}{dt} &= 0.48(V) - \frac{18.1V^2P}{12.9^2 + V^2} \\ \frac{dP}{dt} &= \frac{0.054 \times 18.1V^2P}{12.9^2 + V^2} - 0.49P\end{aligned}$$

where $r = 0.48$, $q = 0.49$, $\beta = 0.054$, $s = 18.1$, and $h = 12.9$. As we have discussed, California sheephead are generalist consumers which feed on benthic invertebrates, including purple sea urchins [19] [20] [28]. It follows, then, that the type III functional response – which incorporates the biological behavior of prey switching, characteristic of generalists – is used in the model that best fits the data according to the second objective function [42]. Our results also suggest that the combination of exponential growth and type III functional response yield the best estimated values, given precise values for each model constant. Using this combination, the growth rate of purple sea urchin is 0.48 and death rate for California sheephead is 0.49, differing from $r, q = 0.35$, which we initially suggested in constructing our models. This indicates that purple sea urchin growth rate and California sheephead death rate are greater in the Channel Island kelp forests than in other locations cited in literature. Using this model we also set the food conversion efficiency rate as 0.054, maximum rate of prey consumption per one predator as 18.1, and the half-saturation constant as 12.9.

Model 2.1 and Model 11.1 are both constructed using logistic growth and a type I function response, but Model 11.1 integrates prey refuge. Then we have Model 2.1 as:

$$\begin{aligned}\frac{dV}{dt} &= 0.35(1 - (V/28.49)V) - 0.32VP \\ \frac{dP}{dt} &= 0.05 \times 0.32VP - 0.35P\end{aligned}$$

and we also have Model 11.1 where:

$$\begin{aligned}\frac{dV}{dt} &= 0.35(1 - (V/28.49)V) - 0.32(V - 0.01)P \\ \frac{dP}{dt} &= 0.05 \times 0.32(V - 0.01)P - 0.35P\end{aligned}$$

such that $r = 0.35$, $q = 0.35$, $\beta = 0.05$, $\alpha = 0.32$, $k = 28.49$, and $v = 0.01$. The only difference between these two models is the subtraction of 0.01 from V in Model 11.1. Setting 0.01 as the constant number of prey protected by refuges yields the best model for all those models containing prey refuge. This result, therefore, indicates that purple sea urchins are taking little refuge in the kelp and rocks in their habitats. Purple sea urchin growth rate and California sheephead death rate are 0.35 which are consistent with the limited research we used to determine these two rate constants [1] [38]. We set the food conversion efficiency rate as 0.05 and the capture efficiency at 0.32, indicating that California sheephead have a greater capture efficiency than food conversion efficiency rate in their system. These models suggest that the carrying capacity of sea urchins per site is 28.49 – or at least this carrying capacity yields the best results in this particular model.

Our results suggest that the combination of exponential growth and type III functional response, and the combination of logistic growth and type I functional response best fits the data out of all of our given models.

7.2 Future Work

Given more time and resources, there are a number of areas we can expand and strengthen our analysis. First, we would like to fit the data to models constructed using ratio-dependence, type II functional response, and type II functional response with prey refuge. In doing so, we can learn more about which models and associated biological assumptions best represent the observed purple sea urchin and California sheephead populations.

We also want to construct models incorporating stochastic environmental factors. As we have discussed, purple sea urchins are subject to decline and increase rapidly due to environmental

changes. Incorporating this kind of behaviour into our model, therefore, may potentially fit our data more accurately. The KFM Program provided us with data including population data for red sea urchins. Modeling the predator-prey relationship between California sheephead and red sea urchins, and comparing these models to those incorporating purple sea urchins may be an interesting extension to this paper. Another next step may be to combine red sea urchin and purple sea urchin data in the model – and model, therefore, the California sheephead population with both sea urchin species. Along these lines, we also want to consider other predators of sea urchins, namely the spiny lobster for which the KFM Program collects population data. In this respect, combining predators into a group, as with prey, may be an interesting comparison to the models we have presented in this paper.

Continuing upon this paper, we want to examine more objective functions that can be used to calculate R^2 . All of our objective functions in this paper are unweighted – and in our work prior to writing this paper we tried weighted objective functions which yielded, however, negative R^2 values. There may be more appropriate objective functions that are better determinants over which models best describe the observed data and which models do not.

Finally, there are more sophisticated methods of determining which parameter values to use in our final analysis [34]. One study used a Simplex subroutine for parameter optimizations [34]. Another method of parameter optimization is the Newton-Raphson method, which involves calculating derivatives and is more involved than that used in the mentioned study [34].

Appendix A

Mathematica Notebook: 6.1 Calculations

Model 6.1 α and β calculations

1985 = 0

0 - 1

Solve[22.05 == (0.35 * 14.47) - (α (14.47 - 0.01)1.19)&&

0.9 == (β * α (14.47 - 0.01)1.19) - (0.35 * 1.19), { β , α }

{{ β → -0.0775073, α → -0.987104}}

1 - 2

Solve[-10.87 == (0.35 * 36.52) - (α (36.52 - 0.01)2.09)&&

-0.32 == (β * α (36.52 - 0.01)2.09) - (0.35 * 2.09), { β , α }

{{ β → 0.0173981, α → 0.309963}}

2 - 3

Solve[-4.25 == (0.35 * 25.65) - (α (25.65 - 0.01)1.77)&&

-0.43 == (β * α (25.65 - 0.01)1.77) - (0.35 * 1.77), { β , α }

{{ β → 0.0143262, α → 0.291465}}

3 - 4

Solve[3.88 == (0.35 * 21.40) - (α (21.40 - 0.01)1.34)&&

-0.03 == (β * α (21.40 - 0.01)1.34) - (0.35 * 1.34), { β , α }

$\{\{\beta \rightarrow 0.121607, \alpha \rightarrow 0.125948\}\}$

4 – 5

Solve $[-4.13 == (0.35 * 25.58) - (\alpha(25.58 - 0.01)1.31) \&\&$
 $-0.29 == (\beta * \alpha(25.58 - 0.01)1.31) - (0.35 * 1.31), \{\beta, \alpha\}]$
 $\{\{\beta \rightarrow 0.0128793, \alpha \rightarrow 0.390576\}\}$

5 – 6

Solve $[-4.61 == (0.35 * 21.15) - (\alpha(21.15 - 0.01)1.02) \&\&$
 $0.12 == (\beta * \alpha(21.15 - 0.01)1.02) - (0.35 * 1.02), \{\beta, \alpha\}]$
 $\{\{\beta \rightarrow 0.0397086, \alpha \rightarrow 0.557094\}\}$

6 – 7

Solve $[-3.5 == (0.35 * 16.54) - (\alpha(16.54 - 0.01)1.14) \&\&$
 $-0.09 == (\beta * \alpha(16.54 - 0.01)1.14) - (0.35 * 1.14), \{\beta, \alpha\}]$
 $\{\{\beta \rightarrow 0.0332652, \alpha \rightarrow 0.492937\}\}$

7 – 8

Solve $[-6.16 == (.35 * 13.04) - (\alpha(13.04 - 0.01)1.05) \&\&$
 $0.31 == (\beta * \alpha(13.04 - 0.01)1.05) - (0.35 * 1.05), \{\beta, \alpha\}]$
 $\{\{\beta \rightarrow 0.0631761, \alpha \rightarrow 0.783832\}\}$

8 – 9

Solve $[5.22 == (0.35 * 6.88) - (\alpha(6.88 - 0.01)1.36) \&\&$
 $0.08 == (\beta * \alpha(6.88 - 0.01)1.36) - (0.35 * 1.36), \{\beta, \alpha\}]$
 $\{\{\beta \rightarrow -0.197724, \alpha \rightarrow -0.300968\}\}$

9 – 10

Solve $[17.11 == (0.35 * 12.10) - (\alpha(12.10 - 0.01)1.44) \&\&$
 $1.18 == (\beta * \alpha(12.10 - 0.01)1.44) - (0.35 * 1.44), \{\beta, \alpha\}]$
 $\{\{\beta \rightarrow -0.130796, \alpha \rightarrow -0.739535\}\}$

10 – 11

$$\text{Solve}[-7.01 == (0.35 * 29.21) - (\alpha(29.21 - 0.01)1.18)\&\&$$

$$0.03 == (\beta * \alpha(29.21 - 0.01)1.18) - (0.35 * 1.18), \{\beta, \alpha\}]$$

$$\{\{\beta \rightarrow 0.0257057, \alpha \rightarrow 0.50016\}\}$$

11 – 12

$$\text{Solve}[-3.5 == (0.35 * 22.20) - (\alpha(22.20 - 0.01)1.21)\&\&$$

$$-0.61 == (\beta * \alpha(22.20 - 0.01)1.21) - (0.35 * 1.21), \{\beta, \alpha\}]$$

$$\{\{\beta \rightarrow -0.0165484, \alpha \rightarrow 0.419741\}\}$$

12 – 13

$$\text{Solve}[-4.97 == (0.35 * 18.70) - (\alpha(18.70 - 0.01)0.60)\&\&$$

$$-0.12 == (\beta * \alpha(18.70 - 0.01)0.60) - (0.35 * 0.60), \{\beta, \alpha\}]$$

$$\{\{\beta \rightarrow 0.00781589, \alpha \rightarrow 1.02684\}\}$$

13 – 14

$$\text{Solve}[8.61 == (0.35 * 13.73) - (\alpha(13.73 - 0.01)0.48)\&\&$$

$$0.68 == (\beta * \alpha(13.73 - 0.01)0.48) - (0.35 * 0.48), \{\beta, \alpha\}]$$

$$\{\{\beta \rightarrow -0.222894, \alpha \rightarrow -0.57777\}\}$$

14 – 15

$$\text{Solve}[24.41 == (0.35 * 22.34) - (\alpha(22.34 - 0.01)1.16)\&\&$$

$$-0.08 == (\beta * \alpha(22.34 - 0.01)1.16) - (0.35 * 1.16), \{\beta, \alpha\}]$$

$$\{\{\beta \rightarrow -0.0196492, \alpha \rightarrow -0.64051\}\}$$

15 – 16

$$\text{Solve}[-18.98 == (0.35 * 46.75) - (\alpha(46.75 - 0.01)1.08)\&\&$$

$$-0.39 == (\beta * \alpha(46.75 - 0.01)1.08) - (0.35 * 1.08), \{\beta, \alpha\}]$$

$$\{\{\beta \rightarrow -0.000339535, \alpha \rightarrow 0.70014\}\}$$

16 – 17

$$\text{Solve}[-7.86 == (0.35 * 27.77) - (\alpha(27.77 - 0.01)0.69)\&\&$$

$$-0.03 == (\beta * \alpha(27.77 - 0.01)0.69) - (0.35 * 0.69), \{\beta, \alpha\}]$$

$$\{\{\beta \rightarrow 0.0120311, \alpha \rightarrow 0.917779\}\}$$

17 – 18

$$\text{Solve}[-11.91 == (0.35 * 19.91) - (\alpha(19.91 - 0.01)0.66)\&\&$$

$$-0.28 == (\beta * \alpha(19.91 - 0.01)0.66) - (0.35 * 0.66), \{\beta, \alpha\}]$$

$$\{\{\beta \rightarrow -0.00259555, \alpha \rightarrow 1.43738\}\}$$

18 – 19

$$\text{Solve}[4.14 == (0.35 * 8) - (\alpha(8 - 0.01)0.38)\&\&0.06 == (\beta * \alpha(8 - 0.01)0.38) - (0.35 * 0.38),$$

$$\{\beta, \alpha\}]$$

$$\{\{\beta \rightarrow -0.14403, \alpha \rightarrow -0.441341\}\}$$

19 – 20

$$\text{Solve}[4.28 == (0.35 * 12.14) - (\alpha(12.14 - 0.01)0.44)\&\&$$

$$-0.03 == (\beta * \alpha(12.14 - 0.01)0.44) - (0.35 * 0.44), \{\beta, \alpha\}]$$

$$\{\{\beta \rightarrow -4., \alpha \rightarrow -0.00580829\}\}$$

20 – 21

$$\text{Solve}[1.27 == (0.35 * 16.42) - (\alpha(16.42 - 0.01)0.41)\&\&$$

$$0.30 == (\beta * \alpha(16.42 - 0.01)0.41) - (0.35 * 0.41), \{\beta, \alpha\}]$$

$$\{\{\beta \rightarrow 0.0990619, \alpha \rightarrow 0.665418\}\}$$

21 – 22

$$\text{Solve}[-0.98 == (0.35 * 17.69) - (\alpha(17.69 - 0.01)0.71)\&\&$$

$$-0.30 == (\beta * \alpha(17.69 - 0.01)0.71) - (0.35 * 0.71), \{\beta, \alpha\}]$$

$$\{\{\beta \rightarrow -0.0071812, \alpha \rightarrow 0.571307\}\}$$

22 – 23

$$\text{Solve}[5.54 == (0.35 * 16.71) - (\alpha(16.71 - 0.01)0.41)\&\&$$

$$0 == (\beta * \alpha(16.71 - 0.01)0.41) - (0.35 * 0.41), \{\beta, \alpha\}]$$

$$\{\{\beta \rightarrow 0.465154, \alpha \rightarrow 0.0450562\}\}$$

23 – 24

$$\text{Solve}[3.33 == (0.35 * 22.25) - (\alpha(22.25 - 0.01)0.41)\&\&$$

$$0.10 == (\beta * \alpha(22.25 - 0.01)0.41) - (0.35 * 0.41), \{\beta, \alpha\}]$$

$\{\{\beta \rightarrow 0.054627, \alpha \rightarrow 0.488847\}\}$

24 – 25

Solve $[-2.36 == (0.35 * 25.58) - (\alpha(25.58 - 0.01)0.51)&&$

$0.51 == (\beta * \alpha(25.58 - 0.01)0.51) - (0.35 * 0.51), \{\beta, \alpha\}]$

$\{\{\beta \rightarrow 0.0608592, \alpha \rightarrow 0.867515\}\}$

25 – 26

Solve $[10.39 == (0.35 * 23.22) - (\alpha(23.22 - 0.01)1.02)&&$

$-0.18 == (\beta * \alpha(23.22 - 0.01)1.02) - (0.35 * 1.02), \{\beta, \alpha\}]$

$\{\{\beta \rightarrow -0.0782148, \alpha \rightarrow -0.0955893\}\}$

Appendix B

Mathematica Notebook: Equilibrium Points

Model 4.4

$$r = 0.48;$$

$$q = 0.49;$$

$$\beta = 0.054;$$

$$s = 18.1;$$

$$h = 12.9;$$

$$\text{GV}[V, P] := rV - \frac{sV^2P}{h^2 + V^2};$$

$$\text{GP}[V, P] := -qP + \frac{sV^2P\beta}{h^2 + V^2};$$

$$\text{matrix44} = \{\{D[\text{GV}[V, P], V], D[\text{GV}[V, P], P]\}, \{D[\text{GP}[V, P], V], D[\text{GP}[V, P], P]\}\}$$

$$\left\{ \left\{ 0.48 + \frac{36.2PV^3}{(166.41 + V^2)^2} - \frac{36.2PV}{166.41 + V^2}, -\frac{18.1V^2}{166.41 + V^2} \right\}, \left\{ -\frac{1.9548PV^3}{(166.41 + V^2)^2} + \frac{1.9548PV}{166.41 + V^2}, -0.49 + \frac{0.9774V^2}{166.41 + V^2} \right\} \right\}$$

$$\text{Solve}[\{\text{GV}[V, P] == 0, \text{GP}[V, P] == 0\}, \{V, P\}]$$

$$\{\{V \rightarrow -12.9344, P \rightarrow -0.684201\}, \{V \rightarrow 0., P \rightarrow 0.\}, \{V \rightarrow 12.9344, P \rightarrow 0.684201\}\}$$

$$\text{matrix44e} = \left\{ \left\{ 0.48 + \frac{36.2 \cdot 0.68 \cdot 12.93^3}{(166.41 + 12.93^2)^2} - \frac{36.2 \cdot 0.68 \cdot 12.93}{166.41 + 12.93^2}, -\frac{18.1 \cdot 12.93^2}{166.41 + 12.93^2} \right\}, \right.$$

$$\left. \left\{ -\frac{1.9548 \cdot 0.68 \cdot 12.93^3}{(166.41 + 12.93^2)^2} + \frac{1.9548 \cdot 0.68 \cdot 12.93}{166.41 + 12.93^2}, -"0.49" + \frac{0.9774 \cdot 12.93^2}{166.41 + 12.93^2} \right\} \right\}$$

$$\{\{0.00405516, -9.07102\}, \{0.025701, -0.00016481\}\}$$

MatrixForm[matrix44e]

$$\begin{pmatrix} 0.00405516 & -9.07102 \\ 0.025701 & -0.00016481 \end{pmatrix}$$

Det[matrix44e]

0.233134

Tr[matrix44e]

0.00389035

0.00389²/4

3.7830249999999997*⁻⁶

Eigenvalues[matrix44e]

{0.00194517 + 0.482835i, 0.00194517 - 0.482835i}

Model 4.7

r = 0.51;

q = 0.47;

β = 0.052;

s = 18.1;

h = 12.9;

GV[V-, P-]:=rV - $\frac{sV^2P}{h^2+V^2}$;

GP[V-, P-]:= -qP + $\frac{sV^2P\beta}{h^2+V^2}$;

matrix47 = {{D[GV[V, P], V], D[GV[V, P], P]}, {D[GP[V, P], V], D[GP[V, P], P]}}

{ {0.51 + $\frac{36.2PV^3}{(166.41+V^2)^2}$ - $\frac{36.2PV}{166.41+V^2}$, - $\frac{18.1V^2}{166.41+V^2}$ }, { - $\frac{1.8824PV^3}{(166.41+V^2)^2}$ + $\frac{1.8824PV}{166.41+V^2}$, -0.47 + $\frac{0.9412V^2}{166.41+V^2}$ } }

Solve[{GV[V, P] == 0, GP[V, P] == 0}, {V, P}]

{{V → -12.8836, P → -0.726962}, {V → 0., P → 0.}, {V → 12.8836, P → 0.726962}}

matrix47e = { {0.51 + $\frac{36.2 \cdot 0.73 \cdot 12.88^3}{(166.41+12.88^2)^2}$ - $\frac{36.2 \cdot 0.73 \cdot 12.88}{166.41+12.88^2}$, - $\frac{18.1 \cdot 12.88^2}{166.41+12.88^2}$ },

{ - $\frac{1.8824 \cdot 0.73 \cdot 12.88^3}{(166.41+12.88^2)^2}$ + $\frac{1.8824 \cdot 0.73 \cdot 12.88}{166.41+12.88^2}$, -0.47 + $\frac{0.9412 \cdot 12.88^2}{166.41+12.88^2}$ } }

{{-0.00292578, -9.03596}, {0.0266721, -0.000130178}}

MatrixForm[matrix47e]

($\begin{pmatrix} -0.00292578 & -9.03596 \\ 0.0266721 & -0.000130178 \end{pmatrix}$ **)**

Det[matrix47e]

0.241009

Tr[matrix47e]

-0.00305596

Eigenvalues[matrix47e]

$\{-0.00152798 + 0.490924i, -0.00152798 - 0.490924i\}$

Model 2.1

$r = 0.35;$

$q = 0.35;$

$\beta = 0.05;$

$\alpha = 0.32;$

$k = 28.49;$

$GV[V, P] := r(1 - (k/V))V - \alpha VP;$

$GP[V, P] := \beta \alpha VP - qP;$

matrix21 = $\{\{D[GV[V, P], V], D[GV[V, P], P]\}, \{D[GP[V, P], V], D[GP[V, P], P]\}\}$

$\{\{-0.32P + 0.35(1 - \frac{28.49}{V}) + \frac{9.9715}{V}, -0.32V\}, \{0.016P, -0.35 + 0.016V\}\}$

Solve $\{\{GV[V, P] == 0, GP[V, P] == 0\}, \{V, P\}$

$\{\{V \rightarrow 21.875, P \rightarrow -0.33075\}, \{V \rightarrow 28.49, P \rightarrow 0.\}\}$

matrix21e = $\{\{-0.320 + 0.35(1 - \frac{28.49}{28.49}) + \frac{9.97}{28.49}, -0.3228.49\},$

$\{0.016 0, -0.35 + 0.016 28.49\}\}$

$\{\{0.349947, -9.1168\}, \{0., 0.10584\}\}$

MatrixForm[matrix21e]

$\begin{pmatrix} 0.349947 & -9.1168 \\ 0. & 0.10584 \end{pmatrix}$

Det[matrix21e]

0.0370384

Tr[matrix21e]

0.455787

Eigenvalues[matrix21e]

{0.349947, 0.10584}

Model 11.1

$r = 0.35;$

$q = 0.35;$

$\beta = 0.05;$

$\alpha = 0.32;$

$k = 28.49;$

$v = 0.01;$

$GV[V, P] := rV \left(1 - \frac{V}{k}\right) - P\alpha(V - v);$

$GP[V, P] := -qP + P\alpha\beta(V - v);$

matrix21 = {{D[GV[V, P], V], D[GV[V, P], P]}, {D[GP[V, P], V], D[GP[V, P], P]}}

{{{-0.32P + 0.35(1 - 0.0351V) - 0.012285V, -0.32(-0.01 + V)}, {0.016P, -0.35 + 0.016(-0.01 + V)}}}

Solve[{GV[V, P] == 0, GP[V, P] == 0}, {V, P}]

{{V → 0., P → 0.}, {V → 21.885, P → 0.253686}, {V → 28.49, P → 0.}}

matrix111e = {{-0.320.254 + 0.35(1 - 0.035 21.89) - 0.012 21.89, -0.32(-0.01 + 21.89)},

{0.016 0.254, -0.35 + 0.016(-0.01 + 21.89)}}}

{{{-0.262113, -7.0016}, {0.004064, 0.00008}}}

MatrixForm[matrix111e]

$\begin{pmatrix} -0.262113 & -7.0016 \\ 0.004064 & 0.00008 \end{pmatrix}$

Det[matrix111e]

0.0284335

Tr[matrix111e]

-0.262033

Eigenvalues[matrix111e]

$$\{-0.131016 + 0.106152i, -0.131016 - 0.106152i\}$$

Bibliography

- [1] Suzanne H. Alonzo, Meisha Key, Teresa Ish, and Alec D. MacCall, *Status of the California Sheephead*, <https://swfsc.noaa.gov/publications/FED/00275.pdf>.
- [2] Todd W. Anderson, *Predator Responses, Prey Refuges, and Density-Dependent Mortality of a Marine Fish*, *Ecology* **82** (2001), 245–257.
- [3] Roger Arditi and Lev R. Ginzburg, *Coupling in predator-prey dynamics: Ratio-Dependence*, *Journal of Theoretical Biology* **139** (1989), 311–326.
- [4] Alan A. Berryman, *The Origins of Predator-Prey Theory*, *Ecology* **73** (1992), 1530–1535.
- [5] Robert K. Cowen, *The effect of sheephead (*Semicossyphus pulcher*) predation on red sea urchin (*Strongylocentrotus franciscanus*) populations: an experimental analysis*, *Oecologia* **58** (1983), 249–255.
- [6] ———, *Sex Change and Life History Patterns of the Labrid, *Semicossyphus pulcher*, across an Environmental Gradient*, *Copeia* **3** (1990), 787–795.
- [7] ———, *Site-specific differences in the feeding ecology of the California sheephead, *Semicossyphus pulcher* (Labridae)*, *Environ Bio Fishes* **16** (1986), 193–203.
- [8] J.M. Cushing, M. Saleem, and A.A. Agostinho, *A Predator Prey Model with Age Structure*, *Journal of Mathematical Biology* **14** (1982), 231–250.
- [9] Paul K. Dayton, *Ecology of Kelp Communities*, *Annual Review of Ecology and Systematics* **16** (1985), 215–245.
- [10] Paul K. Dayton, Mia J. Tegner, Peter B. Edwards, and Kristen Riser, *Sliding baselines, ghosts, and reduced expectations in kelp forest communities*, *Ecological Applications* **8** (1998), 309–322.
- [11] J.H.P. Dawes and M.O. Souza, *A derivation of Holling’s type I, II, and III functional responses in predator-prey systems*, *Journal of Theoretical Biology* **327** (2013), 11–22.
- [12] David Duggins O., James E. Eckman, and Amy T. Sewell, *Ecology of understory kelp environments. II. Effects of Kelp on recruitment of benthic invertebrates*, *Journal of Experimental Marine Biology and Ecology* **143** (1990), 27–45.

- [13] Thomas A. Ebert, Stephen C. Schroeter, John D. Dixon, and Peter Kalvass, *Settlement patterns of red and purple sea urchins (*Strongylocentrotus franciscanus* and *S. purpuratus*) in California, USA*, Marine Ecology Progress Series **111** (1994), 41–52.
- [14] James A. Estes, David O. Duggins, and Galen B. Rathbum, *The Ecology of Extinctions in Kelp Forest Communities*, Conservation Biology **3** (1989), 252–264.
- [15] Michael S. Foster, Daniel C. Reed, Mark H. Carr, Paul K. Dayton, Daneil P. Malone, John S. Pearse, and Laura Rogers-Bennett, *Kelp Forests in California*, Smithsonian Contributions to the Marine Sciences **39** (2013), 115–132.
- [16] Ellen Gilinsky, *The Role of Fish Predation and Spatial Heterogeneity in Determining Benthic Community Structure*, Ecology **65** (1984), 455–468.
- [17] Gotelli Nicholas J., *A Primer of Ecology*, Sinauer Associates, Inc., Sunderland, MA, 1998.
- [18] Michael H. Graham, *Effects of Local Deforestation on the Diversity and Structure of Southern California Giant Kelp Forest Food Webs*, Ecosystems **7** (2004), 341–357.
- [19] Scott L. Hamilton and Jennifer E. Caselle, *Exploitation and recovery of a sea urchin predator has implications for the resilience of southern California kelp forests*, Proceedings Royal Society B **282** (2014).
- [20] Scott L. Hamilton, Jennifer E. Caselle, Coulson A. Lantz, Tiana L. Egloff, Emi Kondo, Seth D. Newsome, Kerri Loke-Smith, II Pondella Daniel J., Kelly A. Young, and Christopher G. Lowe, *Extensive geographic and ontogenetic variation characterizes the trophic ecology of a temperate reef fish on southern California (USA) rocky reefs*, Marine Ecology Progress Series **429** (2011), 227–244.
- [21] SL Hamilton, JE Caselle, JD Standish, DM Schroeder, MS Love, JA Rosales-Casian, and O Sosa-Nishizaki, *Size-selective harvesting alters life histories of a temperate sex-changing fish*, Ecological Applications **17** (2007), 2268–2280.
- [22] Gary W. Harrison, *Comparing Predator-Prey Models to Luckinbill's Experiment with *Dinidium* and *Paramecium**, P Ecology **76** (1995).
- [23] Christopher Harrold and Daniel C. Reed, *Food availability, sea urchin grazing, and kelp forest community structure*, Ecology **66** (1985).
- [24] Jeremy B.C. Jackson, Michael X. Kirby, Wolfgang H. Berger, Karen A. Bjorndal, Louis W. Botsford, Bruce J. Bourque, Roger H. Bradbury, Richard Cooke, Jon Erlandson, James A. Estes, Terence P. Hughes, Susan Kidwell, Carina B. Lange, Hunter S. Lenihan, John M. Pandolfi, Charles H. Peterson, Robert S. Steneck, Mia J. Tegner, and Robert R. Warner, *Historical Overfishing and the recent Collapse of Coastal Ecosystems*, Science **293** (2001), 629–638.
- [25] David J. Kushner and Joshua L. Sprague, *Channel Islands National Park Kelp Forest Monitoring Handbook*, National Park Service, Fort Collins, CO, 2015.
- [26] Steven L. Lima and Lawrence M. Dill, *Behavioral decisions made under the risk of predation: a review and prospectus*, Canadian Journal of Zoology **68** (1990), 618–640.
- [27] Bruce A. Menge, *Indirect Effects in Marine Rocky Intertidal Interaction Webs: Patterns and Importance*, Ecological Monographs **65** (1995), 21–74.
- [28] Fiorenza Micheli, Priyanga Amarasekare, Jordi Bascompte, and Leah R. Gerber, *Including species interactions in the design and evaluation of marine reserves: some insights from a predator-prey model*, Bulletin of Marine Science **74** (2004), 653–669.

- [29] Christian Mulder and Jan A. Hendriks, *Half-saturation constants in functional responses*, *Global Ecology and Conservation* **2** (2014), 161–169.
- [30] National Park Service, *Channel Islands National Park*, National Park Service.
- [31] P. Anders Nilsson, *Predator behaviour and prey density: evaluating density-dependent intraspecific interactions on predator functional responses*, *Journal of Animal Ecology* **70** (2001), 14–19.
- [32] Virginia W. Noonburg, *Ordinary Differential Equations: From Calculus to Dynamical Systems*, The Mathematical Association of America, USA, 2014.
- [33] John S. Pearse, *Ecological Role of Purple Sea Urchins*, *Science* **314** (2006), 940–941.
- [34] P.A. Piana, L.C. Gomes, and A.A. Agostinho, *Comparison of predator-prey interaction models for fish assemblages from the neotropical region*, *Ecological Modelling* **192** (2006), 259–270.
- [35] Daniel C. Reed and Michael S. Foster, *The effects of canopy shadings on algal recruitment and growth in a giant kelp forest*, *Ecology* **65** (1984), 937–948.
- [36] M.L. Rosenzweig and R.H. MacArthur, *Graphical Representation and Stability Conditions of Predator-Prey Interactions*, *The American Naturalist* **97** (1963), 209–223.
- [37] R.J. Rowly, *Settlement and recruitment of sea urchins *Strongylocentrotus* spp. in a sea urchin barren ground and a kelp bed: are populations regulated by settlement or post-settlement processes?*, *Marine Biology* **100** (1989), 485–494.
- [38] *Red Sea Urchin*, <http://safinacenter.org/documents/2012/03/sea-urchin-red-bc-uni-full-species-report.pdf>.
- [39] R.E. Scheinbling and J. Hamm, *Interactions between sea urchins (*Strongylocentrotus droebachiensis*) and their predators in the field and laboratory experiments*, *Marine Biology* **110** (1991), 105–116.
- [40] Oswald J. Schmitz, *Direct and Indirect Effects of Predation and Predation risk in Old-Field Interaction Webs*, *The American Naturalist* **151** (1998), 327–342.
- [41] Irmi Seidl and Clem A Tisdell, *Carrying capacity reconsidered: from Malthus' population theory to cultural carrying capacity*, *Ecological Economics* **31** (1999), 395–408.
- [42] Thomas M. Smith and Robert Leo Smith, *Elements of Ecology*, Pearson Education Inc., Glenview, IL, 2012.
- [43] J. N. M. Smith, C. J. Krebs, A. R. E. Sinclair, and R. Boonstra, *Population Biology of Snowshoe Hares. II. Interactions with Winter Food Plants*, *Journal of Animal Ecology* **57** (1988), 269–286.
- [44] M.E. Solomon, *The natural control of animal populations*, *Journal of Animal Ecology* **18** (1949), 1–35.
- [45] Robert Steneck, M.H. Graham, B.J. Bourque, D. Corbett, J.M. Erlandson, J.A. Estes, and M.J. Tenger, *Kelp Forest Ecosystems: Biodiversity, Stability, Resilience and Future*, *Environmental Conservation* **29** (2002), 436–459.
- [46] M.J. Tegner and P.K. Dayton, *Ecosystem effects of fishing in kelp forest communities*, *Journal of Marine Sciences* **57** (2000), 579–589.
- [47] ———, *El Niño effects on southern California kelp forest communities*, *Advances in Ecological Research* **17** (1987), 243–279.

- [48] M.J. Tegner, P.K. Dayton, P.B. Edwards, and K.L. Riser, *Is there evidence for long-term climatic change in southern California kelp forests?*, California Cooperative Oceanic Fisheries Investigations Reports **37** (1996), 111–126.
- [49] ———, *Large-scale, low-frequency oceanographic effects on kelp forest succession: a tale of two cohorts*, Marine Ecology Progress Series **146** (1997), 117–134.
- [50] M.J. Tegner and P.K. Dayton, *Sea urchins, El Niños, and the long term stability of Southern California kelp forest communities*, Marine Ecology Progress Series **77** (1991), 49–63.
- [51] K.K. Tung, *Topics in Mathematical Modeling*, Princeton University Press, Princeton, NJ, 2007.
- [52] R.L. Vadas and R.S. Steneck, *Zonation of deep water benthic algae in the Gulf of Maine*, Journal of Phycology **24** (1988), 338–346.
- [53] Peter J. Wangersky, *Lotka-Volterra Population Models*, Annual Review of Ecology and Systematics **9** (1978), 189–218.
- [54] Robert R. Warner, *The reproductive biology of the protogynous hermaphrodite *Pimelometopon pulchrum* (Pisces: Labridae)*, Fishery Bulletin **73** (1975), 262–283.
- [55] James M. Watanabe and Christopher Harrold, *Destructive grazing by sea urchins *Strongylocentrotus* spp. in a central California kelp forest: potential roles of recruitment, depth, and predation*, Marine Ecology Progress Series **71** (1991), 125–1991.